KCTD12 PROTEINS REGULATE ULK2 TO CONTROL THE DEVELOPMENT OF ASYMMETRIC HABENULAR NEUROPIL

By

Robert W. Taylor

Dissertation

Submitted to the Faculty of the

Graduate School of Vanderbilt University

in partial fulfillment of the requirements

for the degree of

DOCTOR OF PHILOSOPHY

in

Biological Sciences

August, 2011

Nashville, Tennessee

Approved:

Douglas McMahon, PhD

Charles Hong

Donna Webb

Lilliana Solnica-Krezel

Joshua Gamse

For my eternally supportive family,
Tom, Nan, and Ben
And to my beloved wife,
Katie

ACKNOWLEDGEMENTS

When involved in research pursuits, successful experimenters often claim to be only standing on the shoulders of those oft-referenced giants. While it is true that foundational research is the basis for our understanding of natural world, it is not the giants that need acknowledgement here, but instead, those that held the ladder and allowed me to reach those shoulders.

Foremost, the party responsible for this research is Vanderbilt University and the generous Discovery Grant program, without which many projects like my own that would have difficulty garnering federal support are made possible. The careful administration of my graduate career by the faculty and staff of the Biological Sciences department also deserve many thanks. Especially instrumental in the minutiae of my time at Vanderbilt were administrative staff Roz Johnson and Leslie Maxwell. I would also like to thank Department Chair Charles Singleton, and the Directors of Graduate Studies Douglas McMahon and Katherine Friedman for their superlative efforts at making the department a functional and wonderful arena to pursue a degree.

Academically, there are too many influences to even hope to complete an exhaustive list of responsible parties, but without hesitation, the most supportive and influential scientist in my life is my mentor, Joshua Gamse. Under his tutelage I have learned not only technical skills, but how to be a successful researcher. Also, I would like to thank Lilliana Solnica-Krezel, Douglas McMahon, Charles Hong, Donna Webb, and Bruce Appel, the members of my

dissertation committee whose sage advice gave my research direction. The Vanderbilt zebrafish community has also been instrumental in my growth as a scientist and the success of my project.

Members of the Gamse lab, past and present, have always worked together for the good of the group, so here, I would like to thank Corey Snelson, Joshua Clanton, Caleb Doll, Sataree Khuansuwan, Benjamin Dean, Nancy Borsetti, and Simon Wu for their intellectual contributions to my work. Our research would not be possible without a dedicated staff of support technicians, and Erin Booton, Gena Gustin, and Qiang Xian have allowed us to conduct our work in a professional atmosphere.

A special thanks is deserved by the two incredibly talented and committed undergraduates that I have been fortunate with which to work. Anna Talaga, after helping me work with yeast, is pursuing her own degree at Johns Hopkins, and Jenny Qi, who has always shown the utmost grace and courage in the face of difficult experiments, and is set to pursue her own research goals at UC San Francisco. Thank you both.

On a more personal note, I have been blessed with an astonishing community of friends in Nashville, who have been by my side during my most intense period of personal loss. My family, Tom, Nan, and Ben have also supported me in unimaginable ways, for which I will always be thankful. And finally, I'd like to thank my loving, beautiful wife, Katie, who has tolerated so much, and is beside me still.

TABLE OF CONTENTS

LIST OF FIGURES

Figure Page

CHAPTER I

CHAPTER II

CHAPTER III

LIST OF ABBREVIATIONS

ace	acerebellar mutant
ADE	adenine
AKIP1	A-kinase interacting protein 1
AU	arbitrary units
BCIP	5-bromo-4-chloro-3-indolyl-phosphate
CNS	central nervous system
CTD	carboxy-terminal domain
cxcr4b	chemokine receptor type 4b
dpf	days post-fertilization
FR	fasciculus retroflexus
fsi	*frequent situs inversus* mutant
GFP	green fluorescent protein
Hb	habenular nuclei
Hb:Gal	habenula-specific Gal4 driver line Tg[cfos:Gal4]^{s1019t}
HIS	histidine
hpf	hours post-fertilization
HuC	Hu antigen C
IPN	interpeduncular nucleus
K	Kinase domain
Kctd	K+ channel tetramerization domain-containing protein
LEU	leucine
L/R	left-right
LPM	lateral plate mesoderm
memGFP	membrane-localized green fluorescent protein
MO^{ATG}	start-site blocking morpholino
MO^{spl}	splice-blocking morpholino
MT	myc protein tag
NBT	4-nitro blue tetrazolium
nrp1a	neuropilin1a
NTD	amino-terminal domain
PS	proline-serine rich domain
QDO	quadruple dropout media
RT	room temperature
RT-PCR	reverse transcription polymerase chain reaction
Tg	transgenic line
TRP	tryptophan
UAS	upstream activating sequence
UBE2NL	ubiquitin-conjugating enzyme E2N-like
ulk2	*unc-51-like kinase 2*

CHAPTER I

INTRODUCTION

The Importance of Brain Asymmetry

Most features of the vertebrate body plan display near-perfect bilateral symmetry. However, this bilateral symmetry is broken by both asymmetrical placement of organs (ie: left-sided location of the heart) or asymmetry of paired structures (ie: lobes of the lung, brain hemispheres). Morphological asymmetries can be divided into two categories: antisymmetry refers to left-right (L-R) differences in body plan whose sidedness results from environmental factors during development, while directional asymmetries are L-R differences whose sidedness is also inherited and thus are largely consistent in direction among members of a species or clade (Palmer, 2004). In humans, severe medical conditions, such as congenital heart disease, arise as a result of deviations from stereotypical directional asymmetries (Brueckner, 2007).

The phenomenon of left-right asymmetry has fascinated human cultures for thousands of years. Asymmetry of the brain was once thought to be exclusive to humans, in part because two behaviors of which we are proud, hand usage and language, display sidedness. This notion has been dispelled by an accumulation of data over the last century, demonstrating asymmetric behaviors in many vertebrates and invertebrates. Analysis of many species' behavior

suggests that functional asymmetries stem from an anciently derived specialization of the right side for environmentally motivated behaviors and/or pattern recognition and the left side for self-motivated behaviors and/or detail recognition. Such specialization is thought to increase the efficiency of mental processing, and the consistent direction of asymmetry in social organisms may promote behavior that is predictable to the other members of a group (MacNeilage et al., 2009).

It seems, then, that brain asymmetry is a feature common among vertebrates. Asymmetries of the dorsal diencephalon (epithalamus) have been identified in hagfish, lampreys, cartilaginous fish, bony fish, amphibians, reptiles, and, to a lesser degree, birds and mammals (Braitenberg and Kemali, 1970, Harris et al., 1996, Concha and Wilson, 2001), indicating that asymmetry of the epithalamus may have been an ancestral feature of early vertebrates (Concha and Wilson, 2001). Though a blow to human exceptionalism, these discoveries have been a boon to researchers, as it has allowed model organisms to be employed in the investigation of asymmetric brain development.

Brain Asymmetry in Humans

Though brain asymmetry has long been appreciated in humans, surprisingly few anatomical examples of asymmetry have been described. Despite the fact that the two hemispheres of the human brain are nearly identical in mass, the entire organ is rotated slightly in an anti-clockwise direction which creates a striking asymmetry about the midline. Petalias, cortical protrusions that

deform the inner surface of the skull, occur on the left occipital and the right frontal lobes. This increased width of the right frontal and left occipital lobes causes hemispheric shift across the midline known as the Yakovlevian Torque (LeMay, 1976), a feature that has been confirmed by modern morphometric analysis (Lyttelton et al., 2009).

An especially well-characterized asymmetry in the human brain is the paired lobes of the planum temporale. This region is involved in processing auditory language input, and the left planum is significantly larger in most people. Lateralization of language production was one of the first functional asymmetries to be identified. Broca (1861) and Wernicke (1874) found that language was more severely impaired by tumors or strokes occurring in the left hemisphere. This asymmetry is weakly correlated to both limb use preference (handedness) and gender, the strongest likelihood of left-bias being among right-handed men (Toga and Thompson, 2003).

Several asymmetries were described in a seminal study by Geschwind and Levitsky in 1968. The most striking example concerned a marked asymmetry of the planum temporale, a region on the dorsal surface of the superior temporal gyrus involved in speech production (Geschwind and Levitsky, 1968). They reported that the left planum was larger in 65% of individuals and found only 11% of cases displayed right-sided dominance. Asymmetry of this region is almost certainly influenced genetically, as L-R differences are apparent as early as gestational week 31 (Chi et al., 1977). Left-sided language

orientation is not, however, necessarily correlated with left or right handedness (Moffat et al., 1998).

Adjacent to the planum temporale, and also involved in speech recognition and language generation is the Sylvian fissure. Morphometric analysis has shown that the Sylvian fissure is longer, and its slope gentler in the left hemisphere. Asymmetries in the slope and rostral tilt of these paired structures are well correlated with asymmetries in the planum temporale, which well supports the lateralized nature of language perception and generation (LeMay, 1976).

Several studies have implicated neural asymmetry in neuropathological disorders. Increased symmetry of the planum temporale has been reported in patients with language defecits including reading disorders and dyslexia (Larsen et al., 1990). Reversal of planum temporale asymmetry (that is, a volumetric rightward bias) was also observed in MRI scans of nine out of ten children with developmental dyslexia (Hynd et al., 1990, Morgan and Hynd, 1998). In other studies, the perisylvian area has been implicated in some individual cases of schizophrenia. This region contains the primary auditory cortex, and may be the source of auditory hallucinations commonly observed in schizophrenic patients (Lennox et al., 1999, Petty, 1999). Subtly altered planar asymmetry has been reported in several schizophrenic patients, but these studies remain highly controversial (Crow et al., 1989).

A reduction in brain lateralization has been correlated with affective disorders including depression and schizophrenia. Schizophrenic patients show

more highly symmetrical traits in trials that directly measure neural activity (Jeon and Polich, 2001) and those that use task-based approaches to assess laterality (Asai et al., 2009). Reduction in functional asymmetry of language production areas seems to involve increased activity in the right hemisphere, rather than reduction in the left (Bleich-Cohen et al., 2009).

Degenerative neurological disorders also appear to have an asymmetrical component. MRI studies of elderly patients with Alzheimer's disease have shown an asymmetrical enlargement of the left lateral ventricle (Toga and Thompson, 2003). Also, the degeneration of grey matter in the cortex associated with Alzheimer's disease generally spreads in an asymmetric manner. The spread of atrophy eventually affects both hemispheres, but degeneration is detected earlier, and the loss of grey matter is more severe, in the left hemisphere (Thompson et al., 2003).

Situs inversus, a condition in which all thoracic and visceral asymmetries are perfectly and concordantly reversed, has allowed researchers to study whether neural asymmetry is correlated with asymmetry of the rest of the body. Petalia asymmetries are found to be reversed in such patients, while left-sided dominance of language areas persists (Kennedy et al., 1999). This observation indicates that anatomical asymmetries may be controlled by the same factors determining visceral asymmetries, while functional asymmetries may be the result of environmental cues (Tubbs et al., 2003).

Some developmental neural disorders are frequently observed to afflict the brain unilaterally, underlining the subtly asymmetric features of the

developing brain. One example is the excessive cortical folding and abnormal lamination known as polymicrogyria. This defect can occur in a bilateral, symmetric manner (Barkovich et al., 1999), or as a unilateral malformation (Pascual-Castroviejo et al., 2001), both of which are usually diagnosed following presentation of seizures. One study (Chang et al., 2006) has examined several familial cases of unilateral, right-sided polymicrogyria and speculates that, like the bilateral form, the unilateral form of this disease probably has a heritable basis.

Early speculation that brain lateralization defects afflict individuals presenting developmental dyslexia has sparked modern attempts to establish anatomical causality between decreased asymmetry in language centers of the brain and dysfunction of language. Many studies have reported a reduction of asymmetry in the brains of dyslexics (Galaburda et al., 1985, Humphreys et al., 1990, Duara et al., 1991, Kushch et al., 1993). However, symmetrical anatomy of the brain is thought to be necessary but insufficient to cause reading disorder as up to one-third of healthy individuals can display similar deviations from normal asymmetry (Steinmetz, 1996).

A great deal of effort has been made to elucidate both the molecular underpinnings of asymmetric brain development using genetic model systems and the functional consequences of atypical functional lateralization in human patients. However, at this time, any attempts to marry the two fields are largely speculative. A greater focus on the behavioral consequences of improper asymmetry in model nervous systems and deeper analysis of the development of

human brain lateralization may lead to a day when disorders such as dyslexia and schizophrenia can be predicted by assaying neural laterality.

The Epithalamus: An Accessible "Workshop" to Study Vertebrate Brain Asymmetry

As noted above, asymmetry of the epithalamus (or dorsal diencephalon) is a common feature of hagfish, lampreys, cartilaginous fish, bony fish, amphibians, reptiles, and, to a lesser degree, birds and mammals (Braitenberg and Kemali, 1970, Harris et al., 1996, Concha and Wilson, 2001). Much of the work describing the genetic control of the development of CNS laterality in vertebrates has centered on the zebrafish, both for its well-documented advantages in embryology and genetics, and the presence of robust L/R asymmetries in the epithalamus. Habenular circuitry has also been implicated in schizophrenic presentation (Shepard et al., 2006) and one recent study described a unilateral, right-sided reduction in habenular volume, cell number, and cell area in depressed, but not schizophrenic patients (Ranft et al., 2009).

The zebrafish epithalamus is located posterior to the telencephalon and anterior to the prominent diencephalic optic tecta (Figure 1A, B), and consists of the pineal complex and the bilateral habenular nuclei (Figure 1C).

The pineal complex of zebrafish includes a pineal organ whose stalk emerges from just left of the midline, and a small sister organ called the parapineal, which is found on the left side of the brain. The pineal organ in fish is a photosensitive clock organ that secretes melatonin (Cahill, 1996); the para-

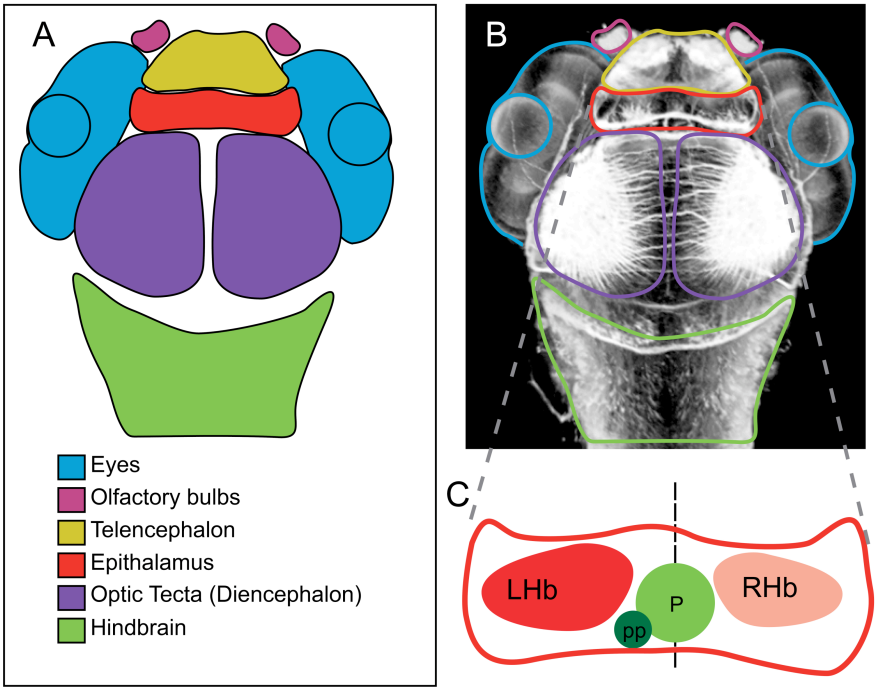

Figure 1. The orientation of the asymmetric zebrafish epithalamus. (A) Schematic representation of the organization of the zebrafish central nervous system (CNS) as viewed from a dorsal perspective at 4 dpf. (B) The organization of the zebrafish CNS as revealed by acetylated tubulin immunofluoresence. (C) Diagram of the asymmetric epithalamus including the pineal, parapineal, and left and right habenular nuclei. Abbreviations: LHb: left habenular nucleus, P: pineal organ, pp: parapineal organ, RHb: right habenular nucleus.

pineal organ's function is not well understood although it also produces melatonin-biosynthetic enzymes (Gothilf et al., 1999).

The habenular nuclei, or habenulae, flank the pineal complex, and are part of an evolutionarily ancient conduction system; both habenulae receive input from the forebrain via the stria medularis and send outputs to the midbrain through the fasciculus retroflexus (Sutherland, 1982) (Figure 2). The habenulae are asymmetric in size, number of subnuclei, and gene expression in many vertebrates, with the most striking asymmetries found in amphibians, lizards, and fish (Concha and Wilson, 2001). In zebrafish, each nucleus is divided into a lateral and a medial subnucleus (Aizawa et al., 2005, Gamse et al., 2005). The lateral subnucleus sends efferents to both dorsal and ventral IPN, while the medial subnucleus exclusively projects to the ventral IPN (Aizawa et al., 2005, Gamse et al., 2005) (Figure 2). In addition, the left habenula of zebrafish contains a larger core of dendrites and a larger lateral subnucleus than the right, and uniquely receives input from parapineal axons (Concha et al., 2000, Aizawa et al., 2005, Gamse et al., 2005), while the right habenula exhibits a larger medial subnucleus than the left, and unilaterally synapses with axons from the olfactory bulb (Aizawa et al., 2005, Gamse et al., 2005, Miyasaka et al., 2009).

In the following sections, we will trace the developmental steps and signals that transform an initially symmetric neuroepithelium into the asymmetric epithalamus.

Directionality of Brain Asymmetry is Linked to Organ Asymmetry

In vertebrates, both the brain and the visceral organs are asymmetric. The Nodal signaling pathway directs and coordinates visceral asymmetry (Shiratori and Hamada, 2006) and in zebrafish, Nodal also plays a crucial role in the directionality of brain asymmetry (Ahmad et al., 2004). The Nodal proteins are a subset of the TGF-beta secreted growth factors, which play an important role during vertebrate gastrulation in mesoderm and endoderm specification and neurectoderm patterning (Shen, 2007).

The role of Nodal in asymmetric development was first appreciated in studies of visceral laterality. During somitogenesis in mouse, chicken, rabbit, frog, and fish, Nodal is expressed in the left LPM, starting at the posterior and moving in a “burning fuse” fashion towards the anterior end (Levin et al., 1995, Lowe et al., 1996, Fischer et al., 2002, Long et al., 2003). Nodal activates expression of itself, the transcription factor Pitx2, and the Nodal extracellular antagonist Lefty (ensuring that Nodal expression is transient) (Solnica-Krezel, 2003). Lefty is also expressed in the ventral midline where it prevents right-sided Nodal signaling (Ohi and Wright, 2007).

Left-sided Nodal expression initiates adjacent to a monociliated endodermal organ, called the node in mouse, Henson’s node in chick, gastrocoel roof plate in frog, and Kupffer’s vesicle in fish (Essner et al., 2002). Directionality of Nodal expression appears to be derived from the movement of these cilia,

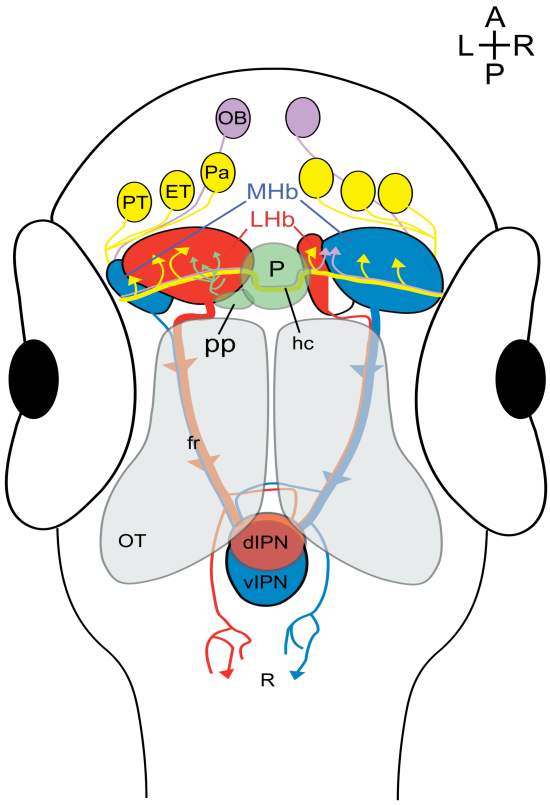

Figure 2. The asymmetric zebrafish habenular nuclei are central to the dorsal diencephalic conduction pathway. Schematic representation of the dorsal diencephalic conduction system. The ratio of lateral (red) to medial (blue) subnuclei is greater in the left habenula, but both sides receive input from both ipsilateral and contralateral neurons of the pallium, the eminentia thalami, and the posterior tuberculum (yellow). The parapineal sends projections only to the left habenula (green), whereas the right habenula receives additional afferents from both olfactory bulbs(purple). Habenular efferents course ventrally to the optic tecta in converging bundles known as the fasciculus retroflexi. Axons originating in the medial subnuclei innervate the ventral region of the interpeduncular nucleus, whereas those of lateral origin can target the dorsal interpeduncular nucleus. Some habenular axons also contact the raphe, just posterior to the interpeduncular nucleus. Abbreviations: dIPN: dorsal interpeduncular nucleus, ET: eminentia thalami, fr: fasciculus retroflexus, hc: habenular commissure, LHb: lateral habenular subnuclei, MHb: medial habenular subnuclei, OB: olfactory bulb, OT: optic tectum, Pa: pallium, P: pineal organ, pp: parapineal organ, PT: posterior tuberculum, R: raphe nucleus, vIPN: ventral interpeduncular nucleus.

although the exact mechanism linking ciliary flow and Nodal expression is not fully understood. In non-mammalian vertebrates, intracellular transport through gap junctions may be the symmetry-breaking event, which is reinforced through ciliary action (Levin, 2004). In either case, a transient calcium release on the left side initiates Nodal expression, which autoactivates its own expression in the LPM (McGrath and Brueckner, 2003).

The side on which Nodal is expressed determines the direction of organ morphogenesis, including the looping of midline structures like the heart and gut, and the placement of unilateral structures including the liver, pancreas, and gall bladder. Expression of Nodal on the right instead of the left in the LPM causes a condition known as situs inversus, in which all organ lateralities are coordinately reversed, while bilateral or absent Nodal in the LPM results in heterotaxia, where laterality of each organ is randomized and is independent of the other organs (Lowe et al., 1996).

The role of Nodal is not restricted to the viscera in teleosts. In medaka and zebrafish, expression of Nodal in the anterior LPM presages a transient pulse of expression in the left epithalamus (Bisgrove et al., 2000, Concha et al., 2000, Liang et al., 2000, Soroldoni et al., 2007) (Figure 3A). In zebrafish, this pulse lasts from 20-24 hours post fertilization. In wild-type embryos, the sidedness of Nodal expression in the brain is coupled with the LPM.

Mutants that affect the formation of Kupffer's vesicle, the ventral midline, or components of the Nodal pathway can cause right sided, bilateral or absent Nodal in the LPM that is reflected in the epithalamus (Bisgrove et al., 2003). No

expression of Nodal has been detected in the brains of other vertebrates, suggesting that it is a derived feature of the teleost lineage (Concha and Wilson, 2001). The way in which the Nodal signal is transmitted from the left LPMm to the epithalamus is assumed to be diffusion, although the existence of a second signal has not been ruled out (Long et al., 2003).

Left-restricted expression of Nodal in the brain depends on the repression of a repressor; in this case the sine oculis related transcription factors Six3b and Six7. When both Six genes are blocked, Nodal expression initiates prematurely and in a wider region of the epithalamus (Inbal et al., 2007). The Six genes act autonomously in the epithalamus and are regulated by a post-transcriptional mechanism that appears to involve Wnt signaling, as an Axin1 hypomorph exhibits a similar phenotype (Carl et al., 2007). Counterintuitively, Nodal, which is expressed in the axial mesoderm during gastrulation, is a prerequisite for Six expression during somitogenesis (Inbal et al., 2007). The model that emerges is one in which early Nodal initiates its own repression by Wnt/Six signaling pathway bilaterally in the brain, then later left-sided Nodal subsequently inactivates Wnt/Six activity unilaterally on the left side. The details of this complex regulatory scheme remain to be uncovered.

Migration of the Asymmetric Parapineal Organ

The parapineal and pineal are derived from a single dorsal-midline-located group of cells in the future epithalamus that can be identified by their expression of the transcription factor *flh* at the end of gastrulation (Concha et al., 2003,

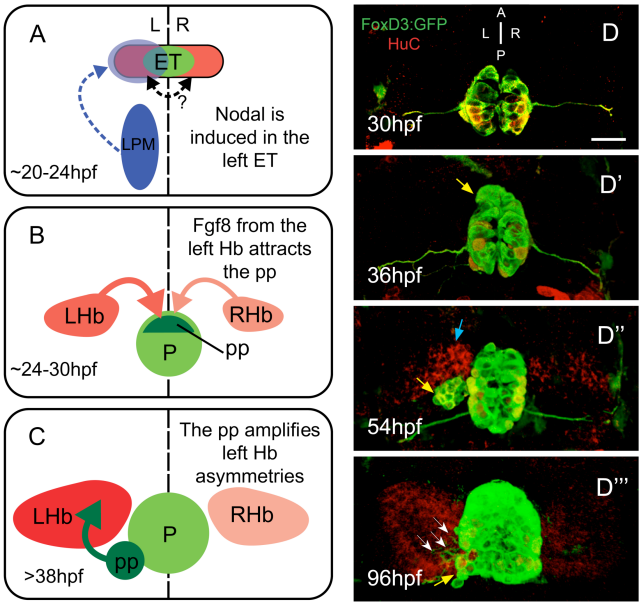

Figure 3. The zebrafish epithalamus develops asymmetrically. (A-C) Model of asymmetric epithalamic development. First, around 20 hours post fertilization (hpf), Nodal expression (blue) in the left lateral plate mesoderm (LPM) activates Nodal expression in the left epithalamus. There may be communication across the midline in the epithalamus (double-headed arrow). At around 24 hpf, a slight left-sided bias of Fgf8 from the habenulae attracts the parapineal. By 38 hpf, the parapineal induces the elaboration of asymmetries only in the left habenula. (D-D'') Timecourse of epithalamic development. Tg*(foxd3:GFP)* (green) marks the pineal and parapineal, and mature neurons are marked with antibodies against HuC (red). (D) At 30 hpf, the pineal is a symmetrical group of neurons centered on the midline. (D') By 36 hpf, the parapineal (yellow arrow) begins to migrate away from the left anterior border of the pineal. (D'') At 54 hpf, the parapineal (yellow arrow) is a distinct accessory organ, and more neurons in the left habenula (blue arrow) have differentiated (i.e. are HuC-positive) than in the right. (D''') The 96 hpf epithalamus is robustly lateralized, with parapineal axons (white arrows) contacting only the left habenula, which is made up of many more HuC-positive neurons than the right.

Gamse et al., 2003). The pineal evaginates from the roof plate, then forms a long stalk which connects a light-sensitive end vesicle to the brain just to the left of the midline (Liang et al., 2000). The parapineal organ precursor cells form a round cluster after budding off from the anterior midline of the *flh*-expressing cluster at 27 hpf, soon after Nodal expression ends. These parapineal precursors then migrate towards the left side of the brain as a string of closely apposed cells (Snelson and Gamse, 2009) (Figure 3B, C, D). Left-sided Nodal signaling in the epithalamus sets the direction in which the parapineal organ migrates and the pineal stalk emerges. The pineal stalk's placement becomes randomized along the left-right axis if Nodal signaling is absent (Liang et al., 2000). Similarly, in mutants with absent or bilateral Nodal expression, the parapineal organ becomes antisymmetric, whereas right-sided Nodal expression causes right-sided placement of the parapineal (Concha et al., 2000, Gamse et al., 2002).

By 48 hpf, the parapineal precursor cells have reached the posterior border of the left habenular nucleus, and begin to send projections anteriorly that will synapse on habenular neurons (Concha et al., 2003). Subsequently, the pineal, parapineal, and habenular nuclei change their relative position: the pineal moves anteriorly relative to the habenular nuclei, while the parapineal cells move ventrally relative to the pineal (Concha et al., 2003). The final arrangement at 4 dpf has a dorsal pineal organ in the midline, while ventrally the habenular nuclei flank the midline and the parapineal is at the posterior edge of the left habenular nucleus.

In addition to its role in directionality of the parapineal, Nodal affects the timing of migration. Mutants that lack Nodal expression in the epithalamus exhibit delayed migration, with a high percentage of parapineal organs remaining in the midline at 48 hpf (Gamse et al., 2002). By 4 dpf, however, the parapineal in these mutants has migrated to the same position as control animals. Mutation of the Wnt pathway scaffolding protein Axin-1 causes a similar delay in migration (Carl et al., 2007).

Asymmetric Neurogenesis in the Habenular Nuclei

Asymmetry in the habenular nuclei, like parapineal migration, is affected by Nodal signaling. A subtle asymmetry in habenular neurogenesis begins just after Nodal signaling ends in the epithalamus. More *cxcr4b*-positive habenular precursor cells are found in the left side of the brain than the right at 28 hpf, and subsequently approximately 25% more HuC positive cells (which have exited the cell cycle) form on the left by 34-38 hpf (Roussigne et al., 2009). Earlier onset of left-sided neurogenesis is supported by BrdU labeling experiments when pulses are administered at 32 hpf (Aizawa et al., 2007). Mutants or drugs which block the Nodal pathway have symmetric HuC expression, as do mutants which result in bilateral Nodal signaling (Roussigne et al., 2009). It remains to be seen if Nodal affects the timing of cell cycle exit or the size of the neurogenic region in the habenular precursors, and whether it acts directly on precursor cells or indirectly by affecting the precursor cell environment. The earliest born habenular neurons contribute to the lateral, Kctd12.1-positive subnucleus of the

habenulae, which will be much larger on the left side. This peaks at 32 hpf; by 36 hpf cells of the medial, Kctd12.2-positive subnucleus (larger on the right) begin to be born, peaking at 48 hpf. Generation of both lateral and medial neurons continues until at least 72 hpf (Aizawa et al., 2007).

Counterintitively, either bilateral or absent Nodal expression seems to reduce the number of precursor cells on the left side, implying that the two sides communicate with one another via a yet-unknown lateral inhibition mechanism (Roussigne et al., 2009). Hyperactivation of Notch signaling betwen 28 hpf and 48 hpf does result in symmetric neurogenesis regardless of Nodal signaling (Aizawa et al., 2007), suggesting that Notch signaling could affect communication between the left and right habenular precursors. These precursors lie adjacent to one another in the subventricular zone prior to dorsal migration and differentiation, and therefore could initiate a signal across the midline via the Notch juxtacrine pathway. Whether Notch is acting in habenular precursors or in another tissue remains to be seen, as Notch pathway components are expressed both in the habenula and in adjacent tissues.

Interaction of the Parapineal and Habenular Nucleus

Recent work has more fully detailed the reciprocal nature of the interaction between migrating parapineal neurons and projection neurons in the habenular nuclei. What was once thought to be a linear cascade of events, beginning with parapineal specification and ending with elaboration of habenular asymmetries,

has now been appreciated as a much more complex interplay between these two groups of developing cells.

Left-sided presence of the parapineal organ serves to amplify asymmetrical features of the left habenula. When the parapineal is ablated by laser surgery, habenular gene expression takes on a more bilaterally symmetric pattern (Gamse et al., 2003, Bianco et al., 2008) and in the absence of a functional parapineal, almost all habenular axons, regardless of left-right origin, innervate the ventral domain of the IPN (Bianco et al., 2008, Snelson and Gamse, 2009). Residual asymmetry in the habenular nuclei following parapineal ablation is likely due to asymmetric neurogenesis initiated by Nodal. Conversely, while the absence of Nodal signaling disrupts the sidedness of laterality, there is no effect on the number of total habenular neurons, asymmetric dendritogenesis or subnucleus formation at 2 dpf and later (Concha et al., 2003, Gamse et al., 2003). Though some habenular asymmetry can be initiated in a parapineal-independent manner, the full array of left-right differences between the two habenulae requires an asymmetrically placed parapineal organ.

The left habenular nucleus attracts the parapineal. Both the left and right habenular nuclei express the secreted signaling ligand Fgf8, while parapineal cells express the *fgfr4* receptor. Parapineal cells in an *fgf8* mutant (*acerebellar*) fail to properly migrate toward the left habenula, indicating that a very subtle asymmetry in Fgf8 may act to tip the balance toward the left habenula(Regan et al., 2009). However, Regan and colleagues found that in *fgf8* mutants (*ace*), a local source of Fgf8 was sufficient to restore leftward parapineal migration,

regardless of the L/R placement of the source. In the absence of asymmetric Nodal signaling and *fgf8* expression, the parapineal migrates towards the source of the exogenous Fgf8 protein (Regan et al., 2009). Notably, a right-sided Fgf bead is insufficient to attract the parapineal to the right in *ace* mutants with intact Nodal signaling. The left-sided initation of neurogenesis by Nodal may bias the parapineal to the left side, perhaps because of earlier or higher expression of a chemoattractant such as Fgf8. Consistent with this idea, ablation of habenular precursors causes parapineal placement to become antisymmetric rather than left-sided (Concha et al., 2003).

The transcription factor Tbx2b is also required for asymmetric placement of the parapineal (Snelson and Gamse, 2009). Tbx2b is expressed within parapineal cells prior to their migration, and likely acts in a cell autonomous fashion. In *tbx2b* mutants, parapineal cells fail to cohere into an anterior cluster; subsequently they migrate posteriorly and ventrally like wild type, but remain at the midline (Snelson and Gamse, 2009). By contrast, parapineal cells in *fgf8* mutants do form a cluster just anterior to the pineal, but never move away from this position (Regan et al., 2009). As the phenotypes of Tbx2b and Fgf8 mutants are not identical, the two molecules either act in different steps of parapineal migration or in parallel pathways. The clustering of parapineal precursors may be a prerequisite for cells to leave the midline in response to chemoattractants from the left habenula.

Signaling between the parapineal and habenular nuclei is an asymmetrically defined system that, in the absence of Nodal signaling from the

LPM, is stochastically oriented. Fgf signaling has been identified as at least one mode of communication from the habenulae to the parapineal, but the nature of parapineal signaling to the left habenula remains unknown, though it is crucial to the establishment of mature habenular asymmetries. Likely candidates for parapineal-habenular communication include canonical Wnt signaling (Carl et al., 2007) and direct synaptic contact.

Differentiation of the Habenular Nuclei

Though habenular asymmetries have been described in many vertebrates (Concha and Wilson, 2001), the asymmetric anatomy of the zebrafish habenulae are certainly the most thoroughly studied. Asymmetries have been described in nearly all aspects of habenular neuroarchitecture including the size of subnuclei, expression of genes, morphology of dendritic processes, and targets of innervation.

The left and right habenulae each consist of both medial and lateral subnuclei (Figure 4A) that describes their position in the adult, which is opposite to their relative positions in the larval brain. In the left habenula, the lateral subnucleus is much larger than the medial, while in the right habenula, cells of the medial subnucleus greatly outnumber those of the lateral. This feature is present into adulthood (Aizawa et al., 2007).

Neuronal morphology also differs a great deal between the left and right Hb. Each Hb subnucleus is made up largely of unipolar neurons with a single axon projecting to the midbrain and a dendritic arbor that colonizes the interior of

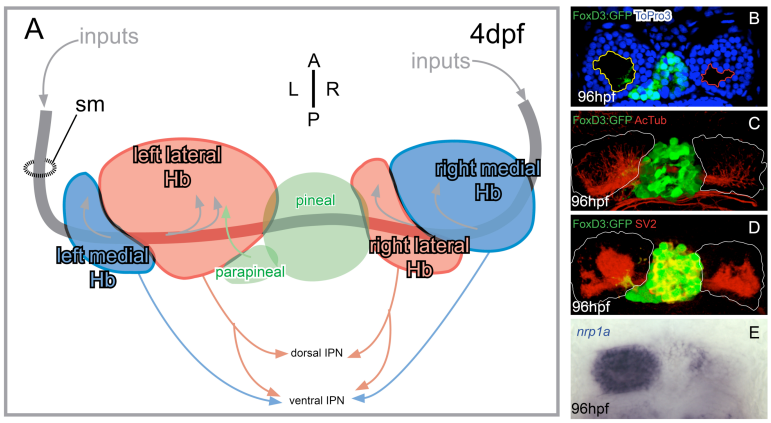

Figure 4. Morphology and gene expression reveal Hb asymmetries. (A) The paired habenular nuclei (Hb) receive input via the stria medullaris (sm) and send efferents to the midbrain target the interpeduncular nucleus (IPN). The asymmetric parapineal organ innervates the left lateral subnucleus (green arrow) and is instrumental in establishing Hb laterality. Each subnucleus is asymmetrically subdivided into medial (blue) and lateral (red) subnuclei, with the lateral subnucleus much larger on the left and the medial subnucleus larger on the right. The nomenclature distinguishing the medial from lateral subnuclei is based on their position in the adult brain, which is the opposite of their position in the 96 hpf larvae shown here. (B) An optical slice through the left and right habenulae at the level of the parapineal stained with the nuclear marker To-Pro3 (blue) demonstrates that the soma-free core of the left habenula (yellow outline) is larger than that in the right (red outline) and is invaded by parapineal axons. (C) The soma-free regions inside each Hb subnucleus are filled with neuronal processes (acetylated tubulin {AcTub}immunofluorescence) including afferent axons and Hb dendrites. The greatest volume of neuropil is found in the large left lateral subnucleus. (D) Antibodies against the presynaptic component SV2 (red) demonstrate a greater density of synaptic contacts in the left habenula. (E) The transcript of the gene encoding the semaphorin co-receptor *neuropilin1a* (*nrp1a)* (blue) is expressed predominantly on the left side in the lateral habenular subnucleus.

the subnucleus. Thus, each subnucleus is a hollow sphere of cell bodies surrounding a soma-free region populated by Hb dendrites and afferent axons. The size of the soma-free region is highly asymmetric with the greatest space on the interior of the left lateral subnucleus (Figure 4B). In addition, the left lateral subnucleus is conspicuously different from the other three subnuclei because by 3dpf, a density of neuropil (representing both Hb dendrites and afferents) develops at the core of this nucleus (Concha and Wilson, 2001) (Fig 4C). The asymmetric nature of habenular afferents is revealed by examination of SV2 labeling (Hendricks and Jesuthasan, 2007), as the left lateral subnucleus is contacted by a much greater density of afferents in a central, soma-free core (Fig 4D). Interestingly, it is this very core of dense neuropil and synapses that is contacted by parapineal axons, making plausible a left-sided specialization for this subnucleus related to circadian input from the pineal complex.

Several gene expression patterns serve as useful molecular markers of habenular asymmetry. *brn3a*, a POU-domain transcription factor is expressed only in neurons of the medial habenulae, and thus in a pattern inverse to that of Kctd12.1. By expressing GFP under *brn3a* regulatory elements, Aizawa and colleagues were able to mark the late-proliferating cells of the right habenula (Aizawa et al., 2005). Members of the *acid-sensing ion channel* gene family are also useful markers of habenular laterality, as *zasic1.1* and *zasic1.3* are both expressed more strongly in the left habenula than in the right (Paukert et al., 2004). Axon guidance co-receptor *neuropilin1a* (*nrp1a*) (Figure 4E) is expressed almost exclusively in the left lateral subnucleus. Nrp1a activity is required for

axons originating in the lateral subnucleus to target the dorsal IPN." (Kuan et al., 2007).

Although asymmetric neurite development has been described qualitatively in several reports (Concha et al., 2000, Concha et al., 2003, Bianco et al., 2008), we developed metrics to quantitatively measure Hb asymmetry. In the zebrafish epithalamus, the L-R asymmetric size ratio of medial and lateral habenular subnuclei can be distinguished based on the distribution of neuronal soma (Figure 5A). During late development, the lateral Hb subnuclei shift dorsal and lateral to the medial subnuclei.

Antibodies against acetylated tubulin mark all axons and dendrites, collectively referred to as neuropil (Figure 5B). The robustly asymmetric distribution of neuropil volume is a defining feature of the asymmetrical zebrafish Hb (arrow in Figure 5 B). To quantitatively describe Hb neurite development, we used image analysis software (Volocity) to precisely determine the neuropil volume in each individual subnucleus (Figure 5 C). The left Hb contains significantly more neuropil than the right ($p=1.34E-7$, $n=12$), owing largely to the contribution of the left lateral subnucleus.

Though some genes are expressed asymmetrically in a transient fashion due to asymmetrical neurogenesis rates (*cxcr4b*/Huc, see above), other expression patterns remain L-R asymmetric into adulthood. Members of the K+ channel tetramerization domain-containing (KCTD) gene family are expressed asymmetrically. *kctd12.1* (previously known as *leftover*) (Figure 6A) is expressed

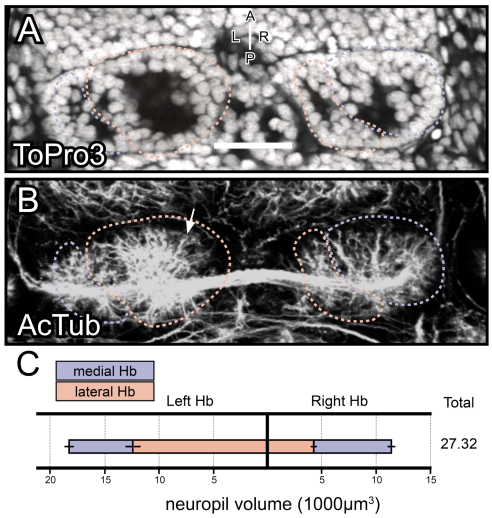

Figure 5. Habenular asymmetries can be quantified by volumetric analysis of acetylated tubulin immunofluorescence. (A)An optical slice through a ToPro3 (nuclear marker)-stained larvae demonstrates asymmetrical subnucleus organization. (B) The soma-free regions inside each Hb subnucleus are filled with neuronal processes (acetylated tubulin {AcTub}immunofluorescence) including afferent axons and Hb dendrites. The greatest volume of neuropil is found in the large left lateral subnucleus (arrow). (C) Volumetric quantification of neuropil volume in each Hb subnuclei. The left lateral subnucleus contains much more neuropil volume than the right, so the total neuropil volume is greater in the left Hb. Scale bars: 50 μm.

in neurons of the lateral subnuclei, and consequently in more cells in the left habenula, while *kctd12.2* (*right on*) (Figure 6B) and *kctd8* (*dexter*) are predominantly expressed in medial subnuclei giving them predominantly right-sided expression patterns (Gamse et al., 2005). Kctd12 protein expression domains correlate nicely with anatomical asymmetries including neuropil density (Figure 5D), and thus habenular Kctd12 expression has been used as a direct readout of direction of asymmetry and relative subnuclei size. However, the function of KCTD proteins in habenular neurons remains mysterious.

The left lateral subnucleus of the Hb may be specialized for particular functions. In support of this idea is the striking segregation of habenular axons originating from different L-R positions. Zebrafish habenular neurons project primarily to the interpeduncular nucleus (IPN), and to a lesser extent to the anterior raphe, in the ventral midbrain (Aizawa et al., 2005, Gamse et al., 2005, Kuan et al., 2007) (Figure 6E). As in other vertebrates, habenular axons reaching the IPN form a series of *en passant* synaptic connections with the IPN (Hamill and Lenn, 1984, Bianco et al., 2008) and strikingly, cross the midline multiple times each. Axons originating from medial subnuclei, which express Kctd12.2, exclusively innervate a dorso-ventrally flattened domain in the ventral aspect of the IPN such that mature axons create a spiraling morphology while restricting themselves to a single plane along the antero-posterior axis (Figure 6F). In sharp contrast, many Kctd12.1+ axons originating from the large left lateral subnucleus adopt a crown-shaped morphology that arcs in the dorso-ventral direction as they cross and recross the midline (Bianco et al., 2008)

(Figure 6F). Thus, differences encoded by the L-R position of habenular neurons is re-encoded in the dorso-ventral segregation of axons at the IPN.

The involvement of habenular neurons in diverse circuits and their laterality in zebrafish has lead several researchers to investigate the behavioral consequences of reversed habenular asymmetry. Barth and colleagues (Barth et al., 2005) studied behavioral reversals in *frequent situs inversus* (*fsi*) mutants in which a high percentage of individuals have a L-R reversal of Hb asymmetry. They found that L-R reversed larvae display a reversal of some behaviors like eye usage when larvae approach their own reflection for the first time and side of bias when adults attack an object. Other lateralized behaviors, like direction of turning when entering a new environment or when startled, were not reversed. Alternatively, Facchin *et al*. (Facchin et al., 2009) found no eye use reversals in *situs inversus* larvae. Both studies are in accord, however, that reversal of brain laterality reduced exploratory behavior and increased latency of emergence into a novel environment. Thus, global reversal of brain laterality may affect behaviors that are not overtly lateralized.

More recently, two groups have begun investigating the role of the zebrafish habenulae in complex behaviors. Agetsuma and colleagues (Agetsuma et al., 2010) tested the flight response to negative stimulus in adult zebrafish expressing the tetanus toxin light chain in neurons of the lateral Hb subnuclei. While control fish initiated rapid turns and increased their speed in response to expectation of shock, animals with compromised Hb circuitry were much more likely to freeze in response to the conditioned stimulus. During

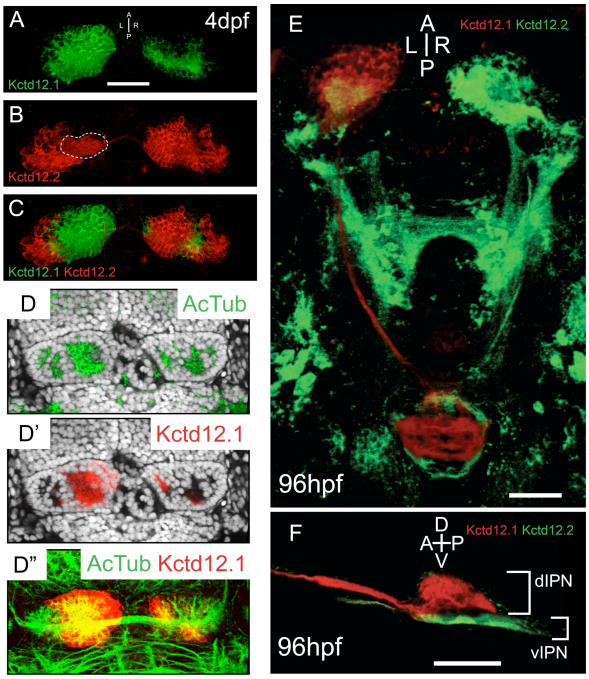

Figure 6. Kctd12 protein expression correlates with morphological asymmetries. (A) Kctd12.1 protein (green) is primarily expressed in lateral Hb subnuclei. (B) Kctd12.2 (red) is expressed in most neurons of the medial Hb subnuclei, (white dashed line indicates signal from dendritic processes, not Kctd12.2-positive soma) (C) in a largely complementary pattern to Kctd12.1. (D) An optical slice through the 96 hpf Hb shows that Kctd12.1 expression in the left lateral subnucleus (red) is tightly correlated with increased neuropil density (green). (E) Dorsal perspective confocal z-projection of Kctd12.1-positive (red) and Kctd12.2-positive (green) neurons coursing from the habenular nuclei to the interpeduncular nucleus via the fasciculus retroflexi. (F) Lateral view of Kctd12.1- and Kctd12.2-positive axons segregated into the dorsal and ventral domains of the interpeduncular nucleus. Scale bars: 50 μm.

training sessions both groups of fish were observed freezing when presented with the conditioned stimulus, but normal fish were able to soon modify their behavior based on previous experience (conditioning) while Hb silenced individuals could not modify their behavior.

Similar experiments have been carried out at larval stages (Lee et al., 2010). In this study, larval zebrafish are trained to avoid a shock by moving to the end of the tank not being illuminated by a red light. Lee and colleagues use two different genetic methods to silence neurons of the Hb and find that even with conditioning, animals with silenced Hb neurons do not cross the tank midline in response to the light, but instead, like in the Agetsuma study, they freeze and do not initiate a flight response. In this paper, the authors note the similarity between the response of Hb-silenced animals and animals that have been conditioned with an unavoidable shock, a model of anxiety. Although the circuitry involved in regulating fear and anxiety behavior is still mysterious, the zebrafish Hb is poised to become a useful model for testing basic genetic factors controlling more complex behaviors.

Discussion

In this study we have attempted to identify the function of Kctd12 proteins in the developing Hb. Though the expression dynamics of Kctd12.1 and Kctd12.2 have been described and characterized, there is, as yet, no functional data concerning the impact that Kctd12 expression has on Hb neurons. Based on the intriguing correlation of Kctd12.1/2 expression with obvious anatomical asymmetries in the

zebrafish epithalamus, we hypothesized that some aspect of Hb asymmetry would rely on the presence and activity of Kctd proteins.

Understanding the role of Kctd proteins in zebrafish Hb neurons could expand our understanding of the development of these crucial nuclei in mammals. Indeed, mining of the Allen Brain Atlas (Lein et al., 2007) reveals that mouse medial habenular cells are specifically enriched for Kctd expression, indicating that similar mechanisms may be acting in Hb neurons of both mammalian and non-mammalian vertebrates. An increased understanding of the development of the habenulo-interpeduncular conduction pathway is similarly vital to our basic understanding of the wiring of the vertebrate CNS.

The paucity of previous study of the function of Kctd12 proteins in Hb neurons is both daunting and exciting. We adopted a strategy for gaining a foothold on this question that relied on non-biased screening of potential protein-protein interaction partners by yeast 2-hybrid screening. The facility of zebrafish genetics would then allow us to take any candidate interactors directly from the biochemical screen to tissue- and organism-level genetic studies. Herein, we describe the fruits of this effort: a novel regulatory mechanism by which Unc-51-like Kinase 2 (Ulk2) acts to promote the elaboration of Hb dendrites, and the discovery that the activity of Ulk2 is negatively regulated by Kctd12 proteins. Our data also indicates that neuropil asymmetry may arise, at least in part, as a result of differential ability of Kctd12.1 and Kctd12.2 to inhibit Ulk2 activity.

CHAPTER II

ULK2 INTERACTS WITH KCTD12.1 AND PROMOTES DENDRITE EXTENSION IN HABENULAR NEURONS

Preface

Portions of this chapter have been accepted for publication in the *Journal of Neuroscience* under the title “Asymmetric Inhibition of Ulk2 causes left-right differences in habenular neuropil formation.” by Taylor et al.

Abstract

The use of Kctd gene and protein expression as markers of epithalamic asymmetry in zebrafish has allowed quite sophisticated genetic studies of the generation of brain asymmetry. Not content to continue the use of these genes purely as markers with no attributable functional data, we set out to gain an initial understanding of the importance of these genes in the development of Hb neurons. Using the yeast 2-hybrid interaction screening system to test millions of proteins for interaction with Kctd12 allowed us to identify Unc-51-like Kinase 2 (Ulk2) as a potential Kctd12 interactor. Here, we confirm this interaction, show that Ulk2 and Kctd12.1 are present together in Hb neurons, and describe the importance of Ulk2 in functional knockdown studies in zebrafish. We find that the presence of Ulk2 is required for normal extension of Hb dendrites, which lays the foundation for Ulk2/Kctd12 genetic interaction studies.

Methods

Zebrafish

Zebrafish embryos were obtained by natural spawning of wild-type AB (Walker, 1999), Tg[*cfos:gal4vp16*]^{s1019t} (referred to here as Hb:Gal)(Scott et al., 2007), Tg[UAS:*kctd12.1:mt*]$^{vu260/264}$, Tg[UAS:*kctd12.1:pA*]^{vu302}, Tg[UAS:*kctd12.2:mt*]^{vu431}, *kctd12.1*^{vu442}, and *kctd12.2*^{fh312} lines. Embryos were raised at 28.5°C on a 14:10 light:dark cycle using standard procedures (Westerfield and ZFIN., 2000), and staged according to hours or days post fertilization (hpf, dpf). For imaging purposes, 0.003% phenylthiourea was added to embryo media to prevent the formation of pigment.

Immunofluorescence

Samples for whole-mount immunohistochemistry were fixed at 96 hpf overnight at room temperature (RT) in Prefer fixative (Anatech) and processed as previously described (Snelson et al., 2008) but without Proteinase K permeabilization. Primary antibodies were incubated at the following concentrations: rabbit anti-Kctd12.1 (1:500)(Gamse et al., 2005), mouse anti-acetylated tubulin (Sigma) (1:500), mouse anti-Myc (Calbiochem) (1:500), rabbit anti-Myc (Sigma) (1:500), mouse anti-GFP (Molecular Probes) (1:500). Primary antibodies were detected using goat-anti-mouse or goat-anti-rabbit secondary antibodies conjugated to either Alexa 488 or Alexa 568 fluorophores (Molecular Probes)(1:300). To visualize cell nuclei, samples were incubated with ToPro 3 (Molecular Probes, 1:1000). Samples were then cleared in glycerol and imaged

with an LSM510 META (Zeiss) confocal microscope with a 40X /1.30 Plan NEOFLUAR oil immersion objective. Z-stacks of the Hb were taken at 1 μm intervals, and extended from the dorsal surface of the larva to the point at which afferents within the stria medullaris enter the Hb, a distance of 60-75 μm. All images were processed using Volocity (Improvision).

Volumetric quantification

To accurately measure neuropil volume in each Hb subnucleus, confocal projections from the dorsal surface of the embryo to the base of the dorsal habenulae in whole mount larvae stained with antibodies against acetylated tubulin were processed using Volocity (Improvision) software. Each Hb subnucleus (left and right, medial and lateral) was individually cropped along morphologically-defined borders. Neuropil volumes were selected using the Intensity Threshold tool in the Volocity measurement software. This tool returns measurements for all individual non-continuous objects, but only the largest continuous volume visually confirmed to correspond to Hb neuropil was selected for further measurement.

To estimate the average dendrite volume per Hb neuron, confocal images of transient scatter-labeled Hb:Gal>memGFP were processed using Volocity (Improvision) software. Regions containing GFP+ clones were cropped and the Intensity Threshold tool was used to determine the continuous volume of GFP signal. These measurements (V_{total}) represent the volume of all dendrites and the soma of labeled cells, but because Hb neurons are unipolar (Bianco et al.,

2008), signal from Hb axons is not included. Estimates for average soma volume ($V_{som\ avg}$ = 268.9μm^3/soma ± 7.29 N=26) were made by carefully outlining isolated soma labeled with memGFP and measuring their volume with the Intensity Threshold tool. With these measurements in hand, the dendrite volume per cell (V_{den}) was estimated as follows: $V_{den} = [V_{total} – (V_{som\ avg}*N)]/N$ where N is the number of neurons in the labeled clone. Statistical analysis consisted of 2-tailed Student's T-tests using Excel (Microsoft).

In situ hybridization

Samples for whole-mount *in situ* hybridization were fixed overnight at 4°C in 4% paraformaldehyde and then dehydrated in methanol at -20°C. Samples were processed as previously described (Thisse and Thisse, 2008). For colorimetric precipitate, samples were developed in a solution of 4-nitro blue tetrazolium (NBT) and 5-bromo-4-chloro-3-indolyl-phosphate (BCIP). Brightfield images of glycerol-cleared samples were captured with a Leica 6000M compound microscope. When combining fluorescent precipitate with immunofluorescent labeling, samples were developed using Fast Red TR/Naphthol (Sigma) and subsequently processed for immunofluorescence.

Yeast 2-hybrid

Potential Kctd12.1 interactors were screened using a commercially available human fetal brain cDNA library (Clontech) fused to the Gal4 activation domain pretransformed into Y187 a-type yeast. A plasmid containing human Kctd12

fused to the Gal4 DNA binding domain was transformed into AH109 α-type yeast. Mating of yeast strains and isolation of interaction-positive colonies were carried out according to the manufacturer's instructions. Subsequent yeast 2-hybrid assays were performed by cotransformation of DNA-binding and activation domain fusion plasmids and plated on interaction-selective media (-ADE, -HIS). The zebrafish homolog of Ulk2 was cloned from cDNA using the primers F: 5'ATGGAGACGGTGGGAGATTT3' and R:5'TTCGTACAGGGTGACGGTG3' and tested in subsequent yeast 2-hybrid assays for interaction with zebrafish Kctd12.1.

Co-immunoprecipitation

MYC:Ulk2 and HA:Kctd12.1 fusion proteins were generated *in vitro* by coupled transcription and translation using the TNT quick coupled transcription translation kit (Promega) according to the manufacturer's instructions. Fusion proteins were then incubated to allow binding without further purification. Fusion protein mixtures were then incubated with antibodies against either Myc of HA epitope tags and subsequently bound to protein A-coated sepharose beads (Pierce). After extensive washing, complexes were released from beads by incubation at 90°C in SDS buffer. Samples were then detected using standard Western blotting on a 4-20% gradient polyacrylamide gel.

Morpholino knockdown of Ulk2

Morpholino antisense oligonucleotides (Gene Tools) were designed to hinder Ulk2 translation by binding to the start site (*ulk2* MO^{ATG} 5'-ATTCAAAATCTCCCACCGTCTCCAT) or to a splice acceptor site at the beginning of exon 7 (*ulk2* MO^{spl} 5'-TCGGCTGTTAAACAAAGAGAGCGCC) resulting in deletion of exon 7 and a frameshift-induced stop codon in exon 8. Morpholinos were resuspended in distilled, deionized water and stored at room temperature. Morpholinos were pressure injected into the yolk of 1-cell stage embryos.

Semiquantitative RT-PCR

Reverse transcription polymerase chain reactions (RT-PCR) were performed on total RNA isolated from 72hpf embryos with Trizol (Invitrogen). Reverse transcription (RT) was performed with random hexameric primers, followed by PCR amplification using primers to amplify sequence from *βactin* (F: 5'-CCATGGATGGGAAAATCGCTGC-3' R: 5'-GTCACACCATCACCAGAGTCC-3'), *ulk2* (F: 5'-CCTTAACAGCAAGGGGATCA-3' R: 5'-ATGCTCCACAGGTCAGCTTT-3'), or *kctd12.1*. Band intensity quantification was carried out with Quantity One (BIO-RAD) software.

Overexpression of Ulk2

ulk2 mRNA was transcribed *in vitro* using the mMessage mMachine transcription kit (Ambion) and pressure injected into 1 cell stage embryos.

Identification and Confirmation of Ulk2 as Kctd12.1 Interactor

In order to assess the function of Kctd12.1 protein in Hb neurons, we used the yeast two-hybrid assay to screen a brain cDNA library to identify protein-protein interactions with Kctd12. The yeast 2-hybrid system is designed to identify and characterize protein-protein interactions. Yeast Gal4 transcription factor is a potent promoter of transcription and is made up of two domains: the DNA-binding domain and the activation domain. The DNA-binding domain is required for binding the upstream activating sequence (UAS), while the activation domain recruites RNA polymerase to begin transcription. The sequence encoding the DNA binding domain and activation domain can be cloned in frame with other genes, generating fusion proteins.

Laboratory yeast strains used in the yeast 2-hybrid are mutant for several genes that causes them to be unable to properly synthesize certain amino acids. In the present screen, these yeast are unable to make adenine and histidine. However, the yeast also carries stable transgenes encoding the genes required for adenine and histidine synthesis under the control of UAS sequences. Therefore, when the cells are grown on media lacking adenine and histidine, they will die. However, if we have introduced a Gal4 DNA-binding domain fused to a protein that interacts with another protein fused to the Gal4 activation domain, an active Gal4 transcription factor can be reconstituted and activate transcription of adenine and histidine biosynthesis genes.

To take advantage of the yeast 2-hybrid system, we tested Kctd12 against a large number of potential interactors without foreknowledge of the constructs

being tested. Because a high-quality zebrafish brain cDNA library is not available, we used the single human homolog of Kctd12.1 and Kctd12.2, HsKCTD12, as bait (fused to the Gal4 DNA binding-domain) and screened a commercially available human fetal brain cDNA library (Clontech). Each library clone was brought into contact with the HsKCTD12 bait construct by large-scale mating. The HhKCTD12 bait was transformed into a haploid a-type yeast strain (AH109), and the clone library were supplied pre-transformed in a haploid α-type yeast strain (YP-187). When a- and α-type yeast are mixed in culture, they mate to produce diploid daughter cells. These progeny were then plated on quadruple-dropout (QDO) media selecting for the both presence of bait and prey plasmids (-LEU, -TRP) and the physical interaction of the bait and prey as indicated by activation of the UAS cassettes (-ADE, -HIS).

By this method, we isolated 66 interaction-positive clones after screening through approximately $2.3x10^6$ library clones. Interacting clones included a-kinase interacting protein 1 (AKIP1), ubiquitin-conjugating enzyme E2N-like (UBE2NL), and several Golgins. Sequence corresponding to Unc-51-like-kinase 2 (Ulk2) was isolated from three independent clones.

Unc-51 was first described in *C. elegans* as an N-terminal serine/threonine kinase required for proper extension of axons (Ogura et al., 1994). The presence of Unc-51 homologues Unc-51-like kinase 1 and 2 (Ulk1 and 2) in a punctate distribution in growing neurites and several genetic studies have revealed an important role of Ulk proteins in the regulation of early

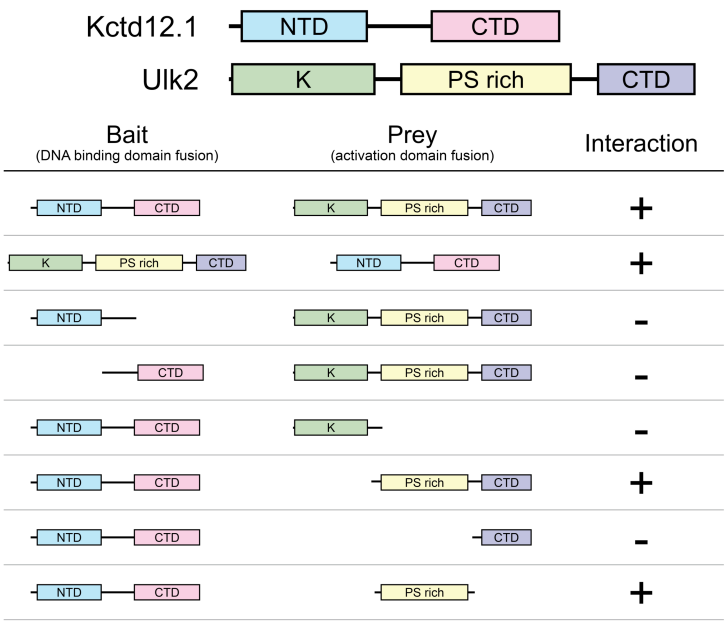

Figure 7. Kctd12.1 Interacts with the Proline-Serine-Rich Region of Ulk2. Kctd12.1 and Ulk2 interact in a yeast 2-hybrid assay. Kctd12.1 is composed of two domains: an N-terminal domain that promotes oligomerization, and a C-terminal domain of undefined function. Ulk2 is composed of 3 domains: an N-terminal serine-threonine kinase domain (K), an internal proline-serine-rich region (PS rich), and a C-terminal domain (CTD) involved in protein-protein interactions. Neither N- nor C- terminal deletions of Kctd12.1 are able to interact with full-length Ulk2. Full-length Kctd12.1 can interact with full-length Ulk2 as well as the proline-serine-rich (PS) domain of Ulk2 alone.

endosome formation (Sann et al., 2009). Early endosomes form a crucial signaling and trafficking center during neurite outgrowth, and thus, Ulk1 and 2 play a major role in the development of neuronal extensions.

First, we confirmed the interaction by testing the zebrafish homologues of Kctd12.1 and Ulk2. After cloning zebrafish Ulk2, we found that, like the human homolog isolated in the screen, zebrafish Ulk2 is able to activate interaction-selection cassettes when co-transformed along with zebrafish Kctd12.1 (Figure 7). In the yeast 2-hybrid system, false positives can result from bait clones that independently recruit transcriptional machinery or prey clones with intrinsic DNA-binding activity can activate selection cassettes even in the absence of interaction with the other protein being tested. To rule out artifactual activation of selection cassettes, we swapped the Gal4 domain that was fused to Ulk2 and Kctd12.1 and found that this combination was still able to interact in yeast (Figure 7).

To gain an initial understanding of structure-function relationships, we tested deletions of the two primary domains of Kctd12.1 for their ability to interact with full-length Ulk2. The N-terminal domain is thought to promote oligomerization of Kctd monomers (Dementieva et al., 2009), and the C-terminal domain has no described function. We found that deletion of either the N-terminal or C-terminal domain of Kctd12.1 abolishes all interaction with full-length Ulk2 (Figure 7). This finding indicates that either the Ulk2 binding site spans both domains or that the binding site on one domain (probably the CTD) requires coordination by the other domain.

To find the region of Ulk2 that interacts with Kctd12.1, we tested prey constructs containing individual domains of Ulk2 for their ability to interact with full-length Kctd12.1. The boundaries of the three primary domains of Ulk2 were determined using protein sequence homology and secondary structure prediction tools. We tested the N-terminal Kinase (K) domain, the internal proline-serine (PS) rich region, and C-terminal domain (CTD) in yeast 2-hybrid assays. Full-length Kctd12.1 is unable to interact with either the K or CTD constructs, precluding either of these domains as the primary binding site for Kctd12.1-Ulk2 interaction (Figure 7). However, by testing the PS domain for interaction with Kctd12.1, we found that this internal domain alone is sufficient for interaction with Kctd12.1 in the yeast 2-hybrid system (Figure 7). Presently, attempts are under way to define the residues involved in this novel interaction with greater resolution.

To verify this interaction by an independent method, we generated HA:Kctd12.1 and MYC:Ulk2 fusion proteins by *in vitro* coupled transcription and translation (Figure 8). We then incubated these tagged proteins, allowing them to bind, and then isolated any complexes formed by further incubation with antibodies directed against either the MYC or HA tag followed by incubation with Protein-A-coated sepharose beads and centrifugation. Co-immunoprecipitates were then released from the beads and analyzed by western blot. Presence of HA:Kctd12.1 in a sample precipitated with antibodies against MYC:Ulk2 and vice versa would confirm an interaction between these two proteins. In these co-immunoprecipitation experiments, we indeed found that MYC:Ulk2 can be

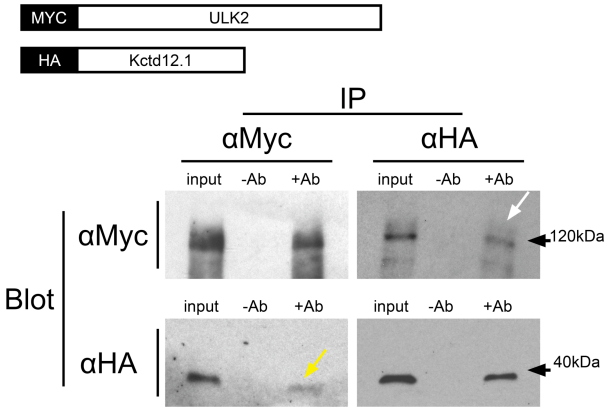

Figure 8. Kctd12.1 and Ulk2 can be co-immunoprecipitated. The interaction between Ulk2 and Kctd12.1 is confirmed by *in vitro* co-immunoprecipitation. After incubation of fusion proteins to allow binding, MYC:Ulk2 could be detected via Western blotting in samples immunoprecipitated with antibodies against HA (white arrow) and likewise, HA:Kctd12.1 was detected upon immunoprecipitation with antibodies against MYC (yellow arrow).

immunoprecipitated along with HA:Kctd12.1 and that HA:Kctd12.1 can likewise be immunoprecipitated along with MYC:Ulk2 (Figure 8). These experiments confirmed that the interaction discovered via yeast 2-hybrid was indeed a relevant interaction and not an artifact of the yeast 2-hybrid technique.

Kctd12.1 and Ulk2 Colocalize in Hb Processes

To consider a Kctd12-Ulk2 interaction relevant to Hb neuropil development, it is imperative to determine whether or not these two proteins come into contact with one another in Hb neurons during a relevant developmental time period. Thus, we set out to analyze the expression of *ulk2* in the developing zebrafish brain. By *in situ* hybridization (Figure 9A-C), we detect *ulk2* mRNA in most neurons of the central nervous system by at least 48 hpf. Expression continues until at least 4 dpf (96 hpf). Broad expression in the brain is consistent with previous reports of broad brain expression patterns in other organisms (Yan et al., 1999). Importantly, we find *ulk2* mRNA bilaterally enriched in Hb neurons as early as 48hpf, and this expression continues until at least 96 hpf. *ulk2* mRNA is expressed in most Hb neurons at higher levels than surrounding telencephalic and diencephalic neurons, and is not consistently enriched asymmetrically in either left or right Hb.

Ulk2 has similar activity to closely-related Ulk1(Sann et al., 2009). Zebrafish have two distinct *ulk1* genes: *ulk1a* and *ulk1b*. We analyzed the expression patterns of these two genes by in situ hybridization. At 2, 3, and 4 dpf, both *ulk1a* (Figure 9 D-F) and *ulk1b* (Figure 9 G-I) are expressed in most

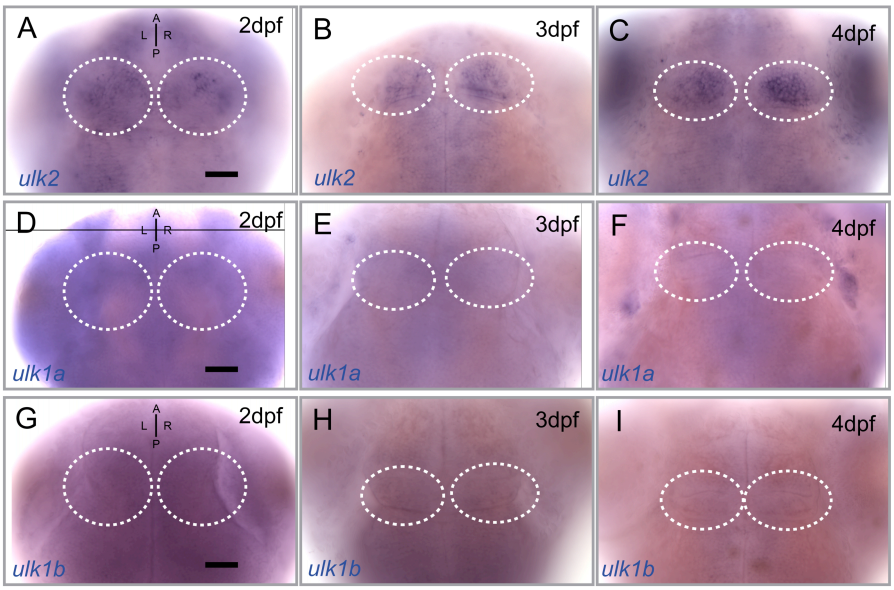

Figure 9. *ulk2*, but not *ulk1a* or *ulk1b* is Enriched in Hb Neurons. (A-C) *ulk2* transcript is detected by *in situ* hybridization in many neurons of the CNS, but is enriched in the paired Hb (white outlines) at 48, 72, and 96 hours post fertilization. (D-I) *ulk1a* (D-F) and *ulk1b* (G-I) transcript are broadly broadly expressed in neurons of the zebrafish CNS, but are not enriched in neurons of the Hb (white outlines). Scale bars: 50 μm.

neurons of the central nervous system. Importantly, unlike *ulk2*, neither *ulk1a* nor *ulk1b* was enriched in neurons of the Hb. Ulk1a and Ulk1b may indeed interact with Kctd12 proteins in the zebrafish Hb, but we pursued genetic studies of Ulk2 based on its enrichment in Hb neurons during development.

Bilateral expression of *ulk2* can be demonstrated by a combination of fluorescent *in situ* hybridization for *ulk2* and immunofluorescence for Kctd12.1 protein. *ulk2* and Kctd12.1 are coexpressed in neurons of the lateral subnucleus of the left Hb, but *ulk2* expression is also found in medial Hb neurons (Figure 10 A-C).

The importance of an interaction between Kctd12 proteins and Ulk2 during Hb development may depend on the cellular compartment in which these two proteins can be found. Therefore, we next wanted to determine the localization of Kctd12.1 and Ulk2 proteins at the subcellular level in Hb neurons. Ulk2 has previously been reported to localize to cytoplasmic puncta in neuronal processes (Zhou et al., 2007). Because no suitable antibody against zebrafish Ulk2 is available, we expressed a GFP:Ulk2 fusion protein in small numbers of Hb neurons by transient transgenesis of a UAS:*gfp*:*ulk2* construct injected into stable Hb:Gal animals (scatter labeling) (Figure 10 D, E). Consistent with previous reports, this fusion protein is present in a punctate pattern in dendritic (arrows, Figure 10E) and axonal processes of Hb neurons, indicating that exogenous GFP:Ulk2 accurately reflects the localization of endogenous Ulk2.

Counterstaining with antibodies against Kctd12.1 shows that GFP:Ulk2 and Kctd12.1 colocalize at the subcellular level (Figure 10 F). Kctd12.1 is

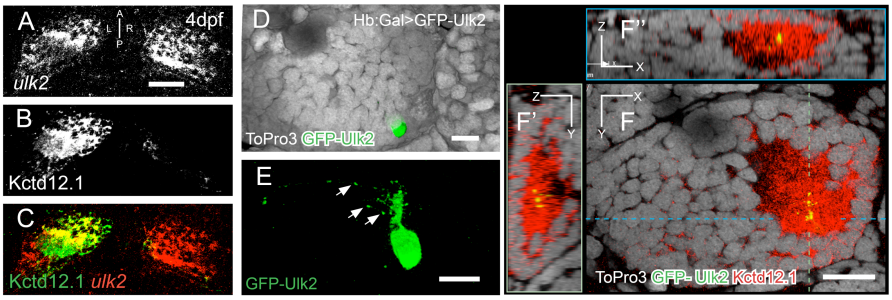

Figure 10. Ulk2 C olocalizes with Kctd12.1. (A-C) A combination of fluorescent *in situ* for *ulk2* transcript and Kctd12.1 immunofluorescence reveals coexpression in the left lateral Hb. (D, E) Transgenic expression of GFP:Ulk2 fusion protein in a single neuron of the left lateral Hb shows localization of GFP:Ulk2 to puncta in Hb dendrites (arrows). (F-F'') GFP:Ulk2 colocalizes with Kctd12.1. The image in (I) is an optical section through the left Hb in (D) with medial to the right and dorsal to the top; dashed lines in (I) indicate the relative orientation of optical sections shown in (I') and (I''). Scale bars in (A) and (D) = 50 µm, in (G-I) = 15 µm.

localized broadly in Hb processes, but the overlap in signal from antibodies against GFP and Kctd12.1 suggests that the two proteins do indeed occupy the same compartment. According to these findings, Ulk2 and Kctd12.1 are present together at a relevant developmental time to affect Hb process development.

Morpholino Knockdown of Ulk2 Inhibits Elaboration of Hb Neuropil

Loss of Ulk activity in both worm and mouse neurons leads to defects in the ability to extend neuronal processes. Ulk kinases are thought to facilitate pro-extension signaling events by promoting the formation of early endosomes near the tips of extending processes. Therefore, we hypothesized that knockdown of Ulk2 in the developing zebrafish embryo could lead to inhibition of neurite elaboration in the developing habenulae. To test the role of Ulk2 in Hb neuron development, we adopted a knockdown strategy using antisense morpholino oligonucleotide (MO) injection. Though Ulk2 morphants have slightly reduced head size and body length (Figure 11 A,B), general neurogenesis is not perturbed. The brains of morphant larvae are generally well-organized with obvious divisions between telencephalon, diencephalon, and hindbrain.

Additionally, motor neurons exit the spinal cord in regular intervals and are able to pathfind into muscle tissue. These observations indicate that Ulk2 depletion by MO injection does not lead to general overall defects in the development of the nervous system (Figure 11 A-B insets). The slight morphological defects ssociated with morpholino injection can be rescued by co-injection of 150pg *ulk2* mRNA (Figure 11 C).

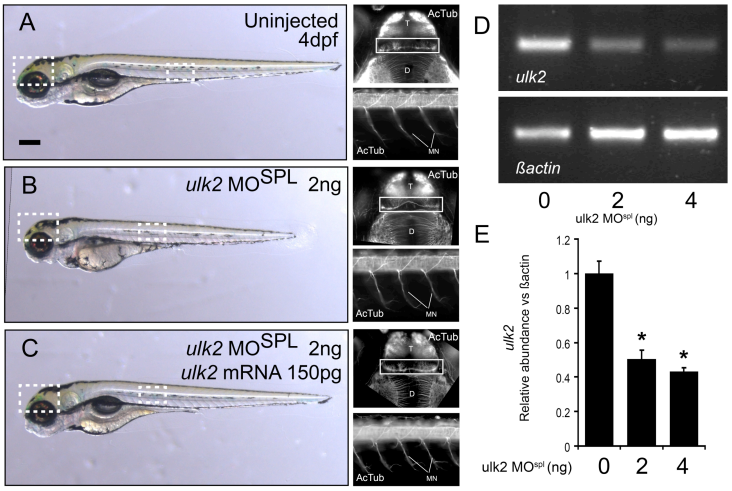

Figure 11. Global Reduction of Ulk2 Levels by Antisense Knockdown. (A-B) Injection of 2 ng *ulk2*MO^{spl} at the one-cell stage produces a mild decrease in head size and body length at 4dpf. The general organization of the central (top insets) and peripheral (bottom insets) nervous system as revealed by acetylated tubulin immunofluoresence is intact in morphant larvae (D: diencephalon, T: telencephalon, MN: motor neurons), but Hb neuropil development (white boxes) is disrupted. (C) Injection of pre-spliced Ulk2 mRNA at the one-cell stage rescues the body length and head size phenotypes of Ulk2 morpholino treatment. (D) The *ulk2* transcript is depleted by morpholino injection. RT-PCR with *ulk2* primers (top panel) shows reduction of *ulk2* mRNA relative to *βactin* (bottom panel) (E) Quantification of band intensity in RT-PCR replicates. 0ng = 1 ± .07 arbitrary units (AU), 2ng = 0.5 ± 0.05 AU, 4ng = 0.43 ± 0.02 AU, N=3. Scale bar = 100 µm.

To assay the effectiveness of morpholino injection at depleting *ulk2* mRNA, we performed RT-PCR using primers within either the *ulk2* or *βactin* coding region on groups of larvae injected with either 0, 2, or 4ng *ulk2*MO^{SPL} and collected at 3 dpf (Figure 11 D). We found that 2 ng *ulk2*MO^{SPL} is sufficient to knock down *ulk2* mRNA to less than 50% of the levels found in WT larvae (quanitified in Figure 11 E), probably through the process of nonsense-mediated decay. Doses of 4 ng lead to severe developmental defects without significantly impacting levels of *ulk2* transcript, suggesting that this dosage level is non-specifically toxic to zebrafish embryos.

To gauge habenular defects in populations of morphant larvae, we separated larvae into three groups based on the morphology of Hb neuropil: WT (Figure 12 A), reduced (Figure 12 B), and absent (Figure 12 C) for population frequency analysis. Samples were categorized in a blinded fashion.

Following treatment with either of two morpholinos complementary to different regions of the *ulk2* mRNA (5 ng *ulk2*MO^{ATG} or 2 ng *ulk2*MO^{SPL}), Hb neuropil is absent (Figure 12 D, white bars) in many larvae (Spl: 65% N=40, ATG: 66.67% N=21). This effect was not elicited by injection of half-maximal doses of either morpholino (2.5 ng *ulk2*MO^{ATG} or 1 ng *ulk2*MO^{SPL} respectively), but co-injection of a mixture of suboptimal morpholino concentrations (2.5 ng *ulk2*MO^{ATG} plus 1 ng *ulk2*MO^{SPL}) was able to effectively inhibit development of Hb neuropil in most larvae (60% N=20), suggesting that both morpholinos target the same transcript.

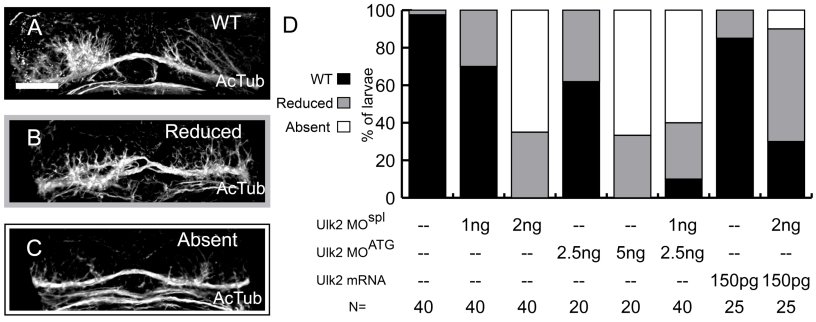

Figure 12. Ulk2 Knockdown Inhibits Development of Asymmetric Hb Neuropil. (A-C) Morphant larvae can be assigned to one of three categories based on the degree of Hb neuropil elaboration. (D) 100% of uninjected larvae have fully elaborated, asymmetric Hb neuropil ("WT" black bars) When injected with either 2 ng *ulk2*MO^{spl} or 5 ng *ulk2*MO^{ATG}, the formation of neuropil in the Hb is inhibited in most larvae (white bars), a phenotype not observed in injections of half-maximal dosage (1 ng and 2.5 ng respectively). Hb neuropil inhibition was also observed when half-maximal doses of each MO were combined, indicating that both morpholinos target the same transcript. Injection of 150pg *in vitro* transcribed *ulk2* mRNA was able to rescue Hb neurite formation when coinjected with 2 ng *ulk2*MO^{spl}. Scale bar = 50 μm.

To confirm that targeting of the *ulk2* transcript is responsible for the Hb neuropil phenotype, we injected synthetic *ulk2* mRNA corresponding to spliced *ulk2* transcript along with 2 ng *ulk2*MO^{SPL}. We found that injection of 150 pg *ulk2* mRNA is able to rescue neuropil development in many 2 ng *ulk2*MO^{SPL} larvae.

In order to discount the possibility that reduction in Hb neuropil in Ulk2 morphants is caused by a loss of Hb neurons, we counted Kctd12.1-positive neurons in larvae treated with 2 ng of *ulk2*MO^{SPL}. Morphants and uninjected larvae did not have significantly different numbers of Kctd12.1-positive neurons (uninjected: 260±7.76, 2 ng *ulk2*MO^{SPL}: 234 ± 8.53, p=0.12 n=12), indicating that loss of Hb neurons is not responsible for the morphant phenotype.

Because measurements of neuropil volume unavoidably include signal from the axons of Hb afferents, we verified that Hb dendrites were specifically affected by Ulk2 knockdown. Injection of a transgenesis vector containing membrane-localized GFP (memGFP) driven by a UAS promoter directly into Hb:Gal embryos results in transient activation of memGFP in Hb neurons in a mosaic fashion. We combined this scatter labeling technique with injection of 2 ng of *ulk2*MO^{SPL} to label small clones of cells in control and *ulk2*MO^{SPL}–injected embryos. We then measured average dendrite volumes in labeled clones. Estimating and subtracting average signal from neuronal soma and dividing by the number of labeled cells allowed us to calculate the average dendrite volume per Hb neuron (Figure 13 A, B). We found that average dendritic volume was significantly reduced in *ulk2* morphants (uninjected: 173.7μm^3 ± 15.6 N=16, 2 ng *ulk2*MO^{SPL}: 131.8 μm^3 ± 11.4 N=16, p=0.028).

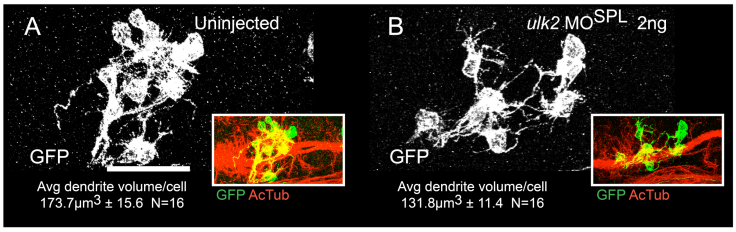

Figure 13. Ulk2 Knockdown Reduces Average Dendrite Volume in Hb Neurons. Mosaic scatter-labeling of Hb neurons with memGFP, followed by average dendrite volume quantification highlights changes in average dendrite volume between uninjected (A) and *ulk2*MO-treated (B) larvae Scale bars = 50 μm.

Discussion

The interesting asymmetric expression patterns of Kctd12 proteins in the zebrafish epithalamus and a paucity of information as to their likely role in developing Hb neurons lead us to use the yeast 2-hybrid screen as a non-biased method to uncover protein-protein interactions involving Kctd12 proteins. We have identified a novel Kctd12.1 interactor, Ulk2, and have subsequently confirmed not only that Kctd12.1 and Ulk2 are able to physically interact, but also that they are both present in Hb neurons during a critical developmental time period.

Our deletion studies indicate that full-length Kctd12.1 is required for the Kctd12.1-Ulk2 interaction, but that the Ulk2 internal PS domain is sufficient for binding. The nature of this interaction can be explored through further Ulk2 PS deletion analysis and by investigation of the structure of the complex through X-ray crystallography. We also hope to determine whether the Ulk2 interaction site spans the two domains of Kctd12.1 or if the interaction simply requires the coordination of one domain by the other. In either scenario, it seems clear that the formation of Kctd12.1 complexes is necessary for the interaction to occur.

Additionally, the discovery of the PS domain as the binding site for Kctd12 proteins leads us to speculate about possible molecular mechanisms at work. Because the PS domain is the site of autophosphorylation required for kinase activity in Ulk2 proteins, it follows that Kctd12 proteins may either sterically or allosterically hinder activation via autophosphorylation.

Our efforts to knockdown Ulk2 protein levels have resulted in an initial understanding of the role of this kinase in Hb development: depletion of Ulk2 causes defects in the extension of Hb dendrites. We were surprised to observe a fairly specific loss of Hb dendrites using a global knockdown strategy. Together with the enrichment of *ulk2* transcript in Hb neurons, these data suggest a Hb-specific role for Ulk2 activity. Ulk2 and Ulk1 are similar both in sequence and in reported roles in autophagy and neurite extension, but while *ulk2* is expressed at higher levels in Hb neurons, *ulk1a* and *ulk1b* expression does not seem particularly upregulated in the Hb. The lack of more global neuronal defects in Ulk2 morphants may be explained by compensation from either Ulk1a, Ulk1b, or both. Complete loss of Ulk2 through identification of a null mutant and investigation into the phenotype of Ulk1a and Ulk1b knockdown may allow the dissection of the level of contribution by the various Ulk homologues.

CHAPTER III

THE PRO-DENDRITOGENESIS ACTIVITY OF ULK2 IS NEGATIVELY REGULATED BY KCTD12 PROTEINS

Abstract

Based on data suggesting that Ulk2 both interacts with Kctd12.1 and significantly affects habnular development, we set out to manipulate Kctd12.1 expression to determine if similar effects on the development of Hb processes could result from either up- or down-regulation of Kctd12 proteins. Because both Kctd12.1 and 12.2 are present in the Hb during critical developmental periods, we developed genetic tools to manipulate both of these proteins. In general, we find that Gal4/UAS-based overexpression of Kctd12 proteins dramatically inhibits the development of Hb neuropil, while mutation of the corresponding genes leads to subtle overdevelopment of Hb dendrites. Additionally, as will be detailed below, our findings suggest that indeed, Kctd12 proteins and Ulk2 act in the same pathway during Hb development, and further, that Kctd12 proteins act to negatively regulate Ulk2, which promotes the extension of Hb dendrites.

Methods

Zebrafish

Zebrafish embryos were obtained by natural spawning of wild-type AB (Walker, 1999), Tg[*cfos:gal4vp16*]^{s1019t} (referred to here as Hb:Gal)(Scott et al., 2007), Tg[UAS:*kctd12.1:mt*]$^{vu260/264}$, Tg[UAS:*kctd12.1:pA*]^{vu302}, Tg[UAS:*kctd12.2:mt*]^{vu431}, *kctd12.1*^{vu442}, and *kctd12.2*^{fh312} lines. Embryos were raised at 28.5°C on a 14:10

light:dark cycle using standard procedures (Westerfield and ZFIN., 2000), and staged according to hours or days post fertilization (hpf, dpf). For imaging purposes, 0.003% phenylthiourea was added to embryo media to prevent the formation of pigment.

Transgenesis

All transgenic animals generated for this study were created using the Tol2kit (Kwan et al., 2007) and built using the Multisite Gateway (Invitrogen) cloning system in the pDestTol2CG2 transgenesis vector. For stable germline transgenics (Tg[UAS:*kctd12.1:mt*]$^{vu260/264}$, Tg[UAS:*kctd12.1:pA*]^{vu302}, Tg[UAS:*kctd12.2:mt*]^{vu431}), AB embryos were injected at late one-cell stage, screened for cardiac GFP at 3dpf, raised to adulthood, and outcrossed to AB animals. For transient scatter-labeling of Hb neurons, Tg[*cfos:gal4vp16*]^{s1019t} (Hb:Gal) embryos were injected with a Tol2 construct containing an upstream activating sequence (UAS) upstream of either Green Fluorescent Protein fused to Ulk2 (*gfp:ulk2*) or a CaaX motif fused to GFP (memGFP) at 2-8 cell stages with the following transmission rates: GFP:Ulk2,1-2%, mGFP 30-50%. Larvae with small clones of labeled Hb neurons were selected for imaging and analysis.

Mutagenesis

The *kctd12.1*^{vu442} mutant was generated by viral insertion that interrupts the *kctd12.1* coding sequence within the N-terminal oligomerization domain.

Homozygous *kctd12.1*^{vu442} mutants are negative for both mRNA by in situ hybridization and protein by immunofluorescence.

The *kctd12.2*^{fh312} mutant was generated by ENU treatment and isolated by TILLING (Draper et al., 2004). This line carries the mutation L74*. Homozygous *kctd12.2*^{fh312} mutants are negative for protein by immunofluorescence.

Immunofluorescence

Samples for whole-mount immunohistochemistry were fixed at 96 hpf overnight at room temperature (RT) in Prefer fixative (Anatech) and processed as previously described (Snelson et al., 2008) but without Proteinase K permeabilization. Primary antibodies were incubated at the following concentrations: rabbit anti-Kctd12.1 (1:500)(Gamse et al., 2005), mouse anti-acetylated tubulin (Sigma) (1:500), mouse anti-Myc (Calbiochem) (1:500), rabbit anti-Myc (Sigma) (1:500), mouse anti-GFP (Molecular Probes) (1:500). Primary antibodies were detected using goat-anti-mouse or goat-anti-rabbit secondary antibodies conjugated to either Alexa 488 or Alexa 568 fluorophores (Molecular Probes)(1:300). To visualize cell nuclei, samples were incubated with ToPro 3 (Molecular Probes, 1:1000). Samples were then cleared in glycerol and imaged with an LSM510 META (Zeiss) confocal microscope with a 40X /1.30 Plan NEOFLUAR oil immersion objective. Z-stacks of the Hb were taken at 1 µm intervals, and extended from the dorsal surface of the larva to the point at which afferents within the stria medullaris enter the Hb, a distance of 60-75µm. All images were processed using Volocity (Improvision).

Volumetric Quantification

To accurately measure neuropil volume in each Hb subnucleus, confocal projections from the dorsal surface of the embryo to the base of the dorsal habenulae in whole mount larvae stained with antibodies against acetylated tubulin were processed using Volocity (Improvision) software. Each Hb subnucleus (left and right, medial and lateral) was individually cropped along morphologically-defined borders. Neuropil volumes were selected using the Intensity Threshold tool in the Volocity measurement software. This tool returns measurements for all individual non-continuous objects, but only the largest continuous volume visually confirmed to correspond to Hb neuropil was selected for further measurement.

Morpholino Knockdown of Ulk2

Morpholino antisense oligonucleotides (Gene Tools) were designed to hinder Ulk2 translation by binding to the start site (*ulk2* MO^{ATG} 5'-ATTCAAAATCTCCCACCGTCTCCAT) or to a splice acceptor site at the beginning of exon 7 (*ulk2* MO^{spl} 5'-TCGGCTGTTAAACAAAGAGAGCGCC) resulting in deletion of exon 7 and a frameshift-induced stop codon in exon 8. Morpholinos were resuspended in distilled, deionized water and stored at room temperature. Morpholinos were pressure injected into the yolk of 1-cell stage embryos.

Semiquantitative RT-PCR

Reverse transcription polymerase chain reactions (RT-PCR) were performed on total RNA isolated from 72 hpf embryos with Trizol (Invitrogen). Reverse transcription (RT) was performed with random hexameric primers, followed by PCR amplification using primers to amplify sequence from *βactin* (F: 5'-CCATGGATGGGAAAATCGCTGC-3' R: 5'-GTCACACCATCACCAGAGTCC-3'), *ulk2* (F: 5'-CCTTAACAGCAAGGGGATCA-3' R: 5'-ATGCTCCACAGGTCAGCTTT-3'), or *kctd12.1*. Band intensity quantification was carried out with Quantity One (BIO-RAD) software.

Overexpression of Ulk2

Synthetic *ulk2* mRNA was transcribed *in vitro* using the mMessage mMachine transcription kit (Ambion) and pressure injected into 1 cell stage embryos.

Overexpression of Kctd12 Proteins Inhibits Hb Neuropil Development

To investigate the impact of Kctd12.1 expression on developing Hb neurons, we overexpressed Kctd12.1 in the Hb of larvae using the Gal4/UAS expression system. Hb:Gal drives expression of Gal4 transcription factor bilaterally in almost all Hb neurons by 4 dpf (Scott et al., 2007) . We generated response lines with transgenes containing a UAS element upstream of a Kctd12.1:Myc tag (MT) fusion protein (Tg[UAS:*kctd12.1-mt*]). When these two transgenes are brought together by crossing Hb:Gal fish with UAS:*kctd12.1-mt* fish, the Gal4 transcription factor produced in Hb neurons by the Hb:Gal transgene binds to the

UAS in the UAS:*kctd12.1-mt* transgene, activating production of a Kctd12.1:MT fusion protein throughout the Hb tissue. In Hb:Gal>Kctd12.1-MT larvae, we detect bilateral *kctd12.1* mRNA and overlapping Myc and Kctd12.1 immunofluorescence (Figure 14 B). Semi-quantitative RT-PCR revealed a doubling in the level of *kctd12.1* mRNA present in double transgenic samples (WT = 1.0 ± 0.11 arbitrary units [AU], Hb:Gal>Kctd12.1-MT = 2.11 ± 0.17 AU, N=3). At 4 dpf, fusion protein was present in almost all Hb neurons. The pattern of Hb neuropil extension in Kctd12.1 overexpression larvae was then assessed by acetylated tubulin immunofluorescence.

When Kctd12.1 is overexpressed in all Hb neurons, the large region of dense neuropil in the left Hb is dramatically reduced (Figure 14 C, D). Larvae with normal levels of Kctd12.1 expression have nearly twice the process volume in the left Hb as compared to the right, but in Hb:Gal>Kctd12.1:MT larvae, only a low volume of neuropil is detected in both habenulae (Figure 14 D). Quantification of neuropil volumes in each subnucleus revealed a significant decrease in neuronal processes in the left lateral ($p=0.0013$, $n=16$) and both left ($p=0.043$, $n=16$) and right ($p=0.046$, $n=16$) medial subnuclei.

There are several explanations of this phenotype that do not include direct effect of the presence of excess Kctd12.1 protein. First, this effect could be a consequence of the exogenous presence of the Myc protein tag, and not an

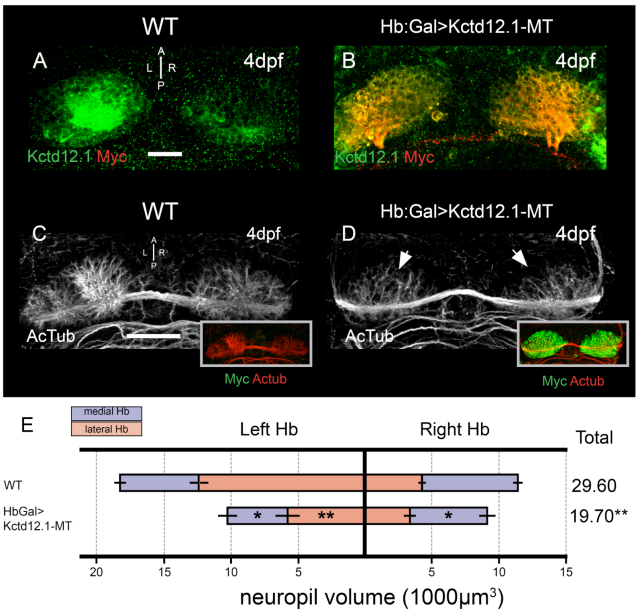

Figure 14. Overexpression of Kctd12.1 Inhibits Elaboration of Hb Neuropil. (A) Kctd12.1 (green) is normally expressed only in Hb neurons of the lateral subnuclei. (B) In Hb:Gal>Kctd12.1-MT larvae, Kctd12.1-MT fusion protein (red) is expressed at high levels in nearly all Hb neurons. (C) WT larvae have an elaborate network of neuropil that segregates within each Hb subnucleus, (D) but the presence of high levels of ectopic Kctd12.1-MT fusion inhibits the elaboration of Hb neuropil. (E) Volumetric quantification of Hb neuropil reduction. Overexpression of Kctd12.1-MT causes significant reduction of total Hb neuropil volume compared to WT (19,693±1,664μm^3 vs 29,602±1,426μm^3, p=0.002, n=16) All subnuclei are significantly affected with the exception of the right lateral subnucleus (asterisks indicate statistical difference compared to WT). Scale bars = 50 μm. *=p<0.05, **=p<0.01, two tailed T-test.

effect of Kctd12.1 itself. Therefore, we generated a separate response transgenic line that contained the *kctd12.1* coding region but did not include the Myc tag (Figure 15 A, B). Hb neuropil defects are not due to an effect of the Myc epitope tag, as overexpression of untagged Kctd12.1 produces an identical Hb neuropil phenotype.

The bilateral reduction in Hb neuropil is a phenotype observed when the parapineal does not form. Overexpression of Kctd12.1 therefore could affect parapineal organogenesis and thus lead to reduced dendritogenesis. To test this possibility, we performed this experiment in another transgenic background, Tg[FoxD3:GFP], which marks the pineal and parapineal (Figure 15 C, D). We determined that the phenotype is not due to parapineal asymmetry defects, as parapineal placement and morphology are normal in double transgenic larvae.

Kctd12.1 and 12.2 share a high level of protein sequence conservation, so we hypothesized that using the same system to overexpress Kctd12.2 would have a similar effect on the development of Hb neuropil. To test this hypothesis, we developed response lines identical to the Tg[UAS:*kctd12.1-mf*] but replaced the *kctd12.1* coding sequence with *kctd12.2* (Figure 16). Like double transgenic Hb:Gal.Kctd12.1-MT larvae, we find that in Hb:Gal.Kctd12.2-MT animals fusion protein is present in nearly all Hb neurons by 4 dpf. Upon analysis of these larvae with acetylated tubulin antibody staining, we observed that neuropil volume is dramatically reduced in larvae that overexpress Kctd12.2-MT. Volumetric quantification of neuropil in Hb:Gal>Kctd12.2-MT reveals significant reductions in neuropil volume in all subnuclei when compared to WT larvae (left

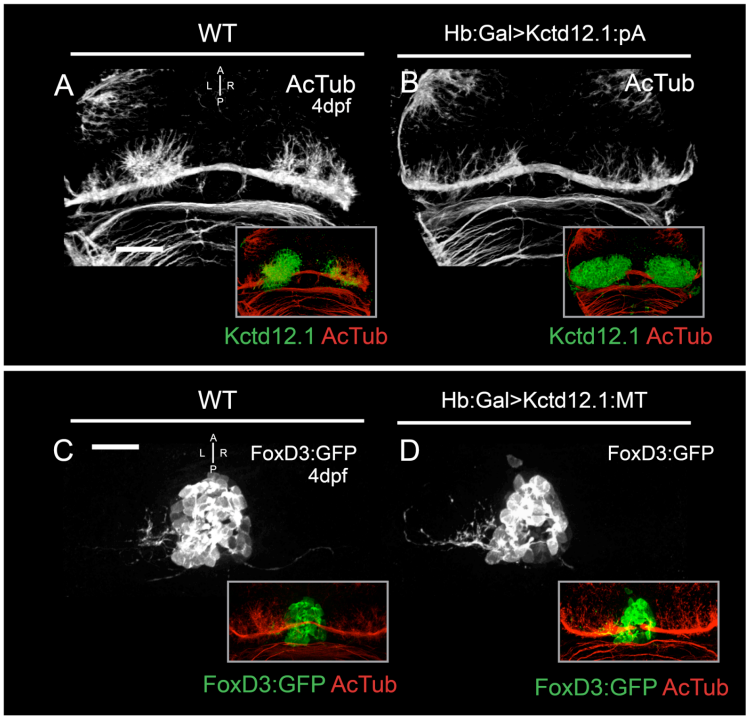

Figure 15. The Reduction in Hb Neuropil in Hb:Gal>Kctd12.1-MT Larvae is Not Caused by Either the Myc Protein Tag or Parapineal Defects. (A) Expression of Kctd12.1 protein (green in insets) is correlated with dense neuropil in the lateral subnucleus of the left Hb in WT larvae. (B) Overexpression of untagged Kctd12.1 in Hb:Gal>Kctd12.1:pA larvae inhibits elaboration of left habenular neuropil in a manner indistinguishable from Hb:Gal>Kctd12.1:MT larvae. (C) At 4dpf in WT larvae, the parapineal, a small, left-sided accessory organ in the pineal complex marked with FoxD3:GFP (green in insets), has innervated the left Hb. (D) In Hb:Gal>Kctd12.1:MT larvae, though Hb neuropil is reduced in the left Hb, placement of the parapineal and axonal targeting of the left Hb are normal. Scale bars = 50mm.

medial: p=1.25E-5, n=16, left lateral: p=8.21E-8, n=16, right lateral: p=1.8E-4, n=16, right medial: p=1.8E-6, n=16,).

In these Gal4/UAS-based overexpression experiments, we observed a dramatic loss of Hb neuropil process extension in Hb neurons that were exposed to elevated levels of Kctd12 proteins during development. This observation lead us to conclude that Kctd12 proteins act as negative regulators of Hb process extension, as they inhibit development of processes when present in overabundance.

Mutation of Kctd12 Genes Leads to Excess Hb Neuropil

Based on the dramatic neuropil reduction when Hb neurons overexpress Kctd12 proteins, we hypothesized that if overexpression of Kctd12 proteins is indeed responsible for the loss of Hb neuropil, then loss of Kctd12 expression through mutation may lead to an excess of Hb neuropil. To test this hypothesis, we made use of a Kctd12.1 null mutant allele, *kctd12.1*^{vu442}, which carries a large viral insertion (Amsterdam et al., 1999) interrupting the *kctd12.1* locus, and a Kctd12.2 mutant allele, *kctd12.2*^{fh312}, which carries an ENU-induced stop codon (L74*) . Both mutations are protein null, with no protein detected by immunofluorescence staining in homozygous mutants (Figure 17 A-D insets), but both alleles are homozygous viable.

We analyzed neuropil volume in single and double homozygous mutant larvae to uncover any subtle differences in neurite volume extension in the absence of Kctd12 proteins. Larvae were visually genotyped by Kctd12 antibody

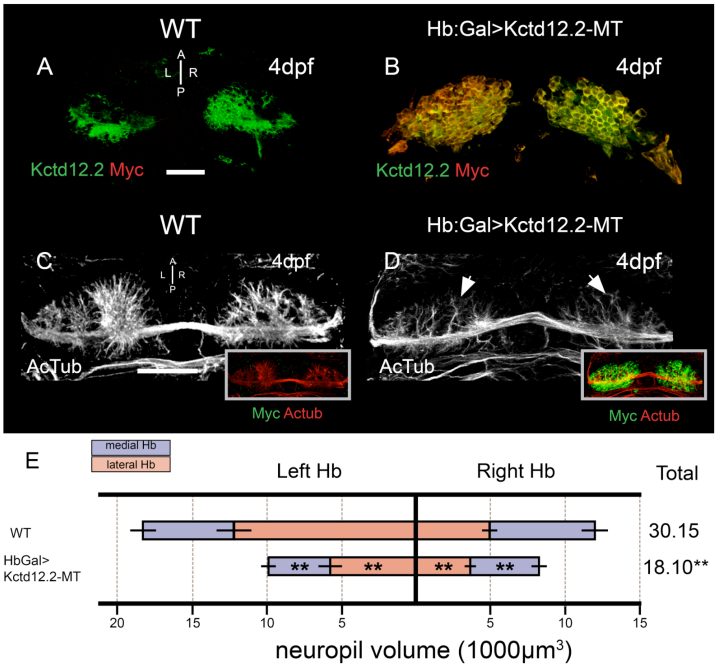

Figure 16. Overexpression of Kctd12.2 Inhibits Elaboration of Hb Neuropil. (A) Kctd12.2 (green) is normally expressed in neurons of the medial subnuclei. (B) In Hb:Gal>Kctd12.2-MT larvae, expression of Kctd12.2-MT fusion protein is driven at high levels in nearly all Hb neurons. (C) WT larvae have an elaborate network of neuropil that segregates within each Hb subnucleus, (D) but the presence of high levels of ectopic Kctd12.2-MT fusion inhibits the elaboration of Hb neuropil. (E) Volumetric quantification of Hb neuropil reduction. Overexpression of Kctd12.2-MT causes significant reduction of total Hb neuropil volume compared to WT (18,103±789μm^3 vs 30,147±2,588μm^3 , p= 7.7E-8, n=16). All subnuclei are significantly affected (asterisks indicate statistical difference compared to WT). Scale bars = 50 μm. *=p<0.05, **=p<0.01, two tailed T-test.

staining pattern. Both Kctd12.1 and Kctd12.2 proteins were labeled in the same fluorescent channel, but homozygosity for the null allele at each Kctd12 locus can be scored based on whether the medial and/or lateral Hb subnuclei are positive for Kctd12 staining. Samples of each genotype were then imaged for acetylated tubulin immunofluorescence and volumetrically analyzed.

In *kctd12.1*^{vu442} homozygotes, we detected a significant increase in neuropil volume in both the left (p=0.0054, N=16) and right (p=0.0039, N=16) lateral Hb subnuclei, as compared to wild type (Figure 17 E). The affected subnuclei are those that express Kctd12.1 in wild type larvae. Similarly, in homozygous *kctd12.2*^{fh312} mutants, quantification reveals excess Hb neuropil in the left medial, right lateral, and right medial subnuclei (p=0.0023, n=16, p=0.000051, n=16, p=0.048, n=16, respectively) (Figure 17 E). Indeed, the only subnucleus unaffected by loss of Kctd12.2 is the left lateral subnucleus, from which Kctd12.2 is normally excluded. Comparison of neuropil between *kctd12.1*^{vu442} and *kctd12.2*^{fh312} single mutants reveals a significantly greater increase in neuropil in *kctd12.1*^{vu442} mutants (p=0.00912, N=16). This finding suggests that Kctd12.2 is a more potent negative regulator of neuropil elaboration than Kctd12.1.

Consistent with the hypothesis that Kctd12.1 and Kctd12.2 proteins negatively regulate neuropil formation in different subnuclei, we found neuropil volumes in *kctd12.1*^{vu442}; *kctd12.2*^{fh312} double mutants to be additively greater

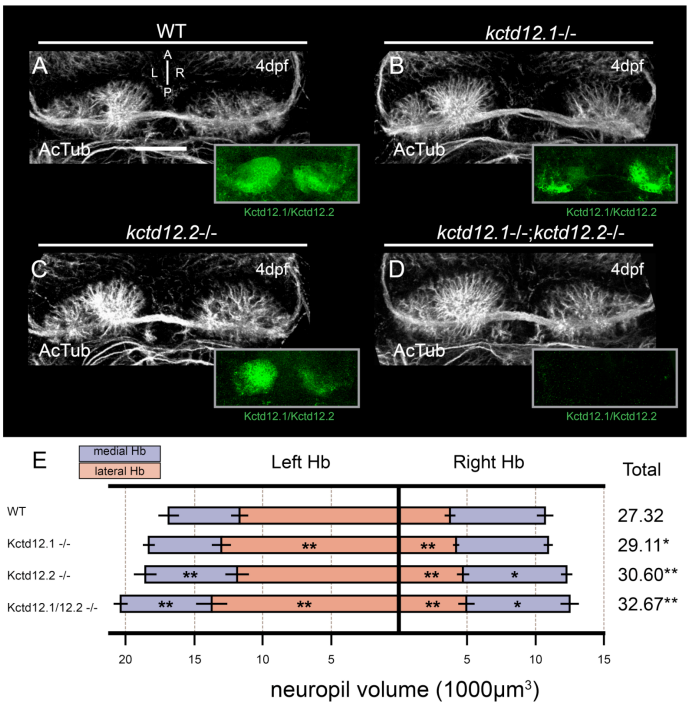

Figure 17. Mutation of Kctd12 Proteins Leads to Excess Hb Neuropil. (A) By 4 dpf, WT larvae display elaborate extension of neuropil in both Hb and express both Kctd12.1 and 12.2 (green, inset). (B) The *kctd12.1* coding sequence is disrupted by a large viral insertion in *kctd12.1*^{vu442} mutants (note lack of Kctd12.1 staining in lateral subnuclei in inset). Hb neuropil in Kctd12.1-negative larvae is slightly expanded in lateral subnuclei. (C) An ENU-induced stop codon in the coding sequence of *kctd12.2* in *kctd12.2*^{fh312} mutants leading to loss of Kctd12.2 protein expression (note lack of Kctd12.2 staining in medial subnuclei in inset). Kctd12.2-negative larvae also display excess elaboration of Hb neuropil, particularly in the medial subnuclei. (D) *kctd12.1*^{vu442}*; kctd12.2*^{fh312} double mutants are negative for both Kctd12 proteins (green, insert) and Hb neuropil is expanded in both the lateral and medial subnuclei. (E) Volumetric quantification of neuropil expansion in *kctd12* mutants. Neuropil expansion is restricted to lateral subnuclei in Kctd12.1-negative larvae, consistent with the expression pattern of Kctd12.1. Neuropil expansion in Kctd12.2-negative larvae affects medial subnuclei as well as the right lateral subnucleus. Double mutant larvae display neuropil expansion in all subnuclei (asterisks indicate statistical difference compared to WT). Scale bars = 50 μm. *=p<0.05, **=p<0.01.

than either single mutant alone, and this increase in neuropil volume affects all Hb subnuclei (Figure 17 E).

Overexpression of Both Kctd12.1 and Ulk2 Can Restore Normal Hb Development

If Kctd12 proteins and Ulk2 operate in the same pathway, as both their interaction and similarity of phenotype suggests, we reasoned that overexpression of Ulk2 should be able to rescue Hb neuropil defects in Hb:Gal>Kctd12.1:MT larvae by restoration of correct relative levels of both proteins in Hb neurons. Specifically, if increased negative regulation of Ulk2 is the primary cause of the loss of neuropil in Kctd12 overexpressors, we should be able to restore the balance of these factors by simultaneously overexpressing Ulk2 itself. To test this hypothesis, we overexpressed Ulk2 by exogenous mRNA injection in the background of Kctd12.1 overexpression (Figure 18). As in previous experiments, overexpression of Kctd12.1-MT leads to dramatic loss of Hb neuropil volume compared to controls (Figure 18 A, B). Conversely, we find that injection of 500pg *ulk2* mRNA leads to a modest increase in Hb neuropil volumes, particularly in medial subnuclei (Figure 18 C). This subtle increase in neuropil volume in response to exogenous Ulk2 protein further supports the idea that Ulk2 acts to promote the extension of neurites.

In agreement with our hypothesis, when exogenous *ulk2* mRNA is administered to Hb:Gal>Kctd12.1:MT embryos, we find that total Hb neuropil volume is restored to levels both qualitatively and statistically indistinguishable from WT ($p=0.072$, $n=8$) (Figure 18 D). In these experiments, overexpression of

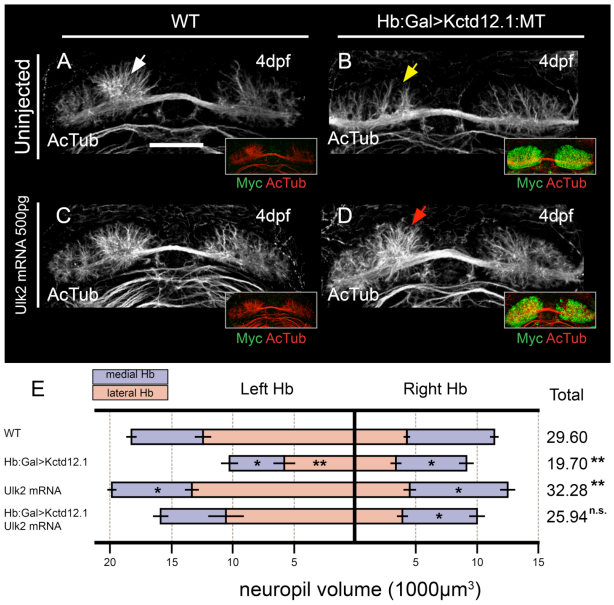

Figure 18: Overexpression of Ulk2 by mRNA Injection Rescues Neuropil Reduction Caused by Kctd12.1 Overexpression. (A) The large volume of neuropil present in the left Hb of wild type larvae (white arrow), (B) is reduced (yellow arrow) by overexpression of Kctd12.1-MT (green in insets) and (C) is slightly increased by injection of 500pg *ulk2* mRNA alone. (D) Injection of 500pg *ulk2* mRNA restores relatively normal neuropil volume in the left Hb (red arrow) of larvae overexpressing Kctd12.1-MT. (E) Volumetric quantification of neuropil phenotype. Overexpression of Kctd12.1-MT significantly reduces neuropil volume in the left lateral and both medial Hb subnuclei. Injection of *ulk2* mRNA slightly increases neuropil volume in the medial subnuclei. Injection of *ulk2* mRNA into Kctd12.1-MT overexpression larvae restores wildtype neuropil volumes to all subnuclei with the exception of the right medial subnucleus (asterisks indicate statistical difference compared to WT). Scale bar = 50 μm. *=p<0.05, **=p<0.01.

Kctd12.1 inhibits endogenous Ulk2 activity to an inappropriate degree, but providing high levels of exogenous Ulk2 can overcome this inhibition and reestablish normal Ulk2-dependent dendrite outgrowth. Indeed, rescue of the Kctd12.1 overexpression phenotype by Ulk2 overexpression, combined with evidence of a direct Ulk2-Kctd12 interaction, leads us to conclude that these two factors are, in fact, part of the same regulatory pathway. However, this experiment does nothing to order these molecules in the pathway. With only these data in hand, it is impossible to distinguish whether Kctd12 proteins regulate Ulk2 or vice versa.

Ulk2 Depletion is Epistatic to Kctd12.1 Mutation

Based on reported roles of Ulk2 as a positive regulator of neurite outgrowth and the excessive neurites in *kctd12* mutants, we hypothesized that Kctd12 proteins negatively regulate the activity of Ulk2 kinase, which positively regulates neuropil formation. To test this hypothesis, we attempted to carry out an epistasis experiment to order the interactions in a pathway. We examined the phenotype of *kctd12.1*^{vu442} treated with an Ulk2 morpholino (Figure 19). In this experiment, the most downstream factor should produce the same phenotype when depleted singly as is evident when both factors are depleted. Thus, if Kctd12 activity is upstream of Ulk2, we expect the Hb neuropil of mutant/morphant larvae to resemble that of Ulk2 knockdown alone.

Mutation of Kctd12.1 in the context of Ulk2 morpholino treatment (2 ng of *ulk2*2 MO^{spl}) results in severely reduced neuropil elaboration relative to WT or

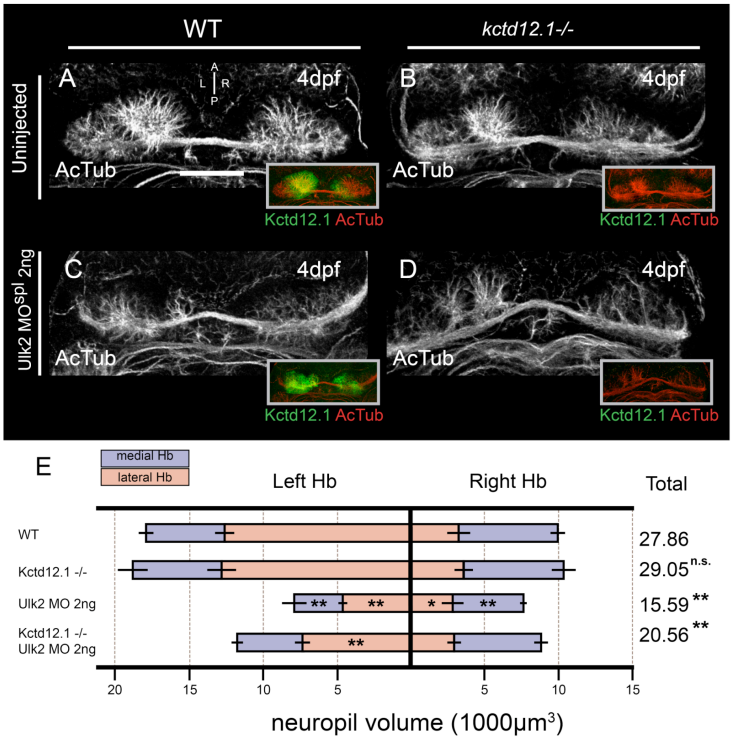

Figure 19: Ulk2 Depletion is Epistatic to Kctd12.1 Mutation. (A) Compared to normal Hb, (B) neuropil development (white arrow) is slightly expanded in homozygous null *kctd12.1* mutant animals (note absence of Kctd12.1 [green] in insets at right). (C) Reduced neuropil (yellow arrow) in the left Hb as a result of Ulk2 antisense depletion (D) also occurs (red arrow) when Ulk2 is depleted in a Kctd12.1 homozygous mutant, indicating that Ulk2 depletion is largely epistatic to mutation of Kctd12.1. (E) Volumetric quantification of Hb neuropil phenotype. Total neuropil volume is significantly reduced following injection of *ulk2* MO^{spl} in either a wild type or Kctd12.1 mutant background (asterisks indicate statistical difference compared to WT). Scale bar = 50 µm. *=p<0.05, **=p<0.01.

mutation of Kctd12.1 alone (Figure 19 A-E). Because the phenotype of the mutant/morphants more closely resemble the phenotype of Ulk2 knockdown alone, it is likely that Ulk2 is downstream in the pathway. In other words, it is likely that Kctd12.1 is regulating Ulk2, which is, in turn, regulating neuropil extension.

Interpretation of this experiment is made more difficult because of the incomplete nature of Ulk2 morpholino knockdown. Because some Ulk2 protein is still produced and active in these fish, neurites still extend to some degree. Confirmation of this epistasis experiment will require the acquisition of *ulk2* null mutants to both confirm the phenotype of Ulk2 morpholino knockdown presented here, and to unambiguously order these two molecules in the development of Hb neuropil.

Discussion

With a strong interaction candidate in hand, we set out to explore the effect of a Kctd12-Ulk2 interaction within the context of a developing embryo. Thanks to the genetic accessibility of the zebrafish, we were able to manipulate the expression of these two proteins in both directions both individually and together. The near total loss of Hb neurites in the presence of high levels of exogenous Kctd12 protein first indicates that Kctd12 proteins must act in a negative regulatory way. This finding was confirmed by the observation that mutation of these two genes leads to a subtle, but significant increase in the volume of neuropil generated by

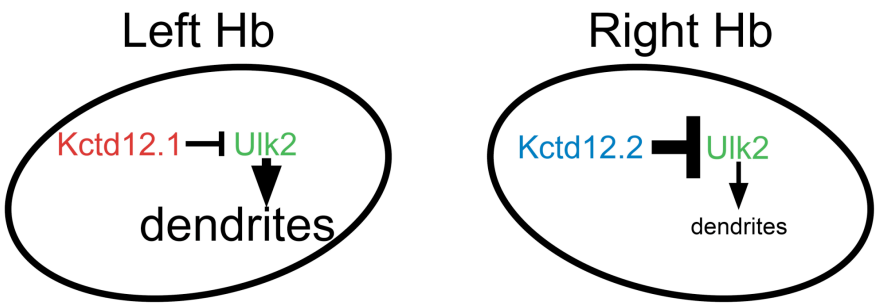

Figure 20. Model of Proposed Regulatory System Resulting in Asymmetric Habenular Neuropil Extension. Ulk2 kinase acts bilaterally to promote elaboration of Hb neuropil, but is negatively regulated by Kctd12 proteins. Asymmetry in neuropil may arise from the greater relative potency of Kctd12.2 acting in medial subnuclei.

Hb neurons. We then confirmed that Kctd12 proteins and Ulk2 are indeed in the same pathway by simultaneously manipulating the expression of each molecule. We found that it is possible to rescue the loss of Hb neuropil in Kctd12 overexpressors by concomitant overexpression of Ulk2 protein. The level to which excess Ulk2 is present, and over what developmental period, is unknown. However, the restoration of Hb neuropil is sufficient to surmise that excess Ulk2 is present at levels sufficient to counteract the presence of excess Kctd12.1.

We have also made an attempt to order these genes in a pathway. Although a classical epistasis experiment cannot be properly executed without a null mutation at the *ulk2* locus, we have simulated this state with morpholino injection. When knockdown of Ulk2 is combined with a Kctd12.1 null mutant, the resulting embryos more closely resemble the phenotype of Ulk2 knockdown alone. This finding leads us to conclude that Kctd12 proteins are upstream of Ulk2 in the regulation of Hb neuropil. The model that emerges has Ulk2 acting to promote the extension of Hb dendrites, while Kctd12 proteins act to inihibit or limit the pro-dendrite activity of Ulk2 (Figure 20). Validation of this model, however, awaits the identification of an *ulk2* null allele.

CHAPTER IV

CONCLUSIONS AND FUTURE DIRECTIONS

The proper development of the highly-conserved habenulo-interpeduncular circuit is crucial to the appropriate regulation of both dopaminergic and serotonergic systems. Using the genetically facile zebrafish as a model of Hb development makes possible the transition from basic molecular interaction screening to organ-level developmental studies. In this study, we have identified a potential protein-protein interaction important for Hb development via yeast 2-hybrid screening and then pursued these findings directly in a vertebrate model system. The novel findings in this work are relevant to both the cell biology of neurite extension and the tissue-level development of asymmetric connectivity in the vertebrate brain.

We have described that Ulk2 and Kctd12 proteins antagonistically regulate the development of Hb neuronal processes. Specifically, Ulk2 promotes neuropil outgrowth and Kctd12.1 is a negative regulator of Ulk2 activity. Overall, the following conclusions can be drawn from this body of work: 1) Kctd12.1 physically interacts with the internal proline-serine rich domain of Ulk2, 2) Ulk2 knockdown and Kctd12 overexpression can both inhibit neuropil formation, 3) loss of Kctd12 expression and overexpression of Ulk2 lead to enhanced elaboration of Hb neuropil, 4) Ulk2 and Kctd12 proteins are in the same pathway, and 5) Ulk2 depletion is epistatic to Kctd12 mutation. This is a previously

uncharacterized interaction that may open a new line of inquiry into the fine control of neurite extension in the developing vertebrate nervous system.

The interaction between Kctd12.1 and Ulk2 is previously unreported. Work in both worms (Ogura et al., 1994) and fuit flies (Toda et al., 2008) has defined a role for Unc 51 kinases in the process of neurite extension, but no mutant phenotype has been described for Kctd mutations in either organism. We find that the Kctd12-Ulk2 interaction is conserved between humans and zebrafish, so it will be interesting to see if this mechanism for regulating dendritogenesis is conserved in invertebrates.

The Ulk2-Kctd12 Interaction May Define a Novel Ulk Regulatory System

We were surprised to find that the minimal domain of Ulk2 required for interaction with Kctd12.1 is the internal PS domain. Using structure prediction algorithms to find candidate interaction sites within the PS domain yielded no homology to previously-reported protein-protein interaction domains. Indeed, based on the enrichment of proline residues, this region is predicted to be highly disordered. Therefore, we have set out to test progressively smaller deletions of this domain for ability to interact with Kctd12.1. The fact that Kctd12.1 seems to bind the portion of Ulk2 that must be phosphorylated to promote Ulk2 activity leads us to speculate that Kctd12.1 may regulate Ulk2 activity by inhibition of Ulk2 phosphorylation. Confirmation of this idea would first require the development of an *in vitro* Ulk2 auto-phosphorylation assay and the subsequent

comparison of phosphorylation rates in the presence and absence of Kctd12.1 complexes.

The structure of Kctd proteins is still poorly understood. Our finding that Kctd12.1-Ulk2 interaction is abolished by deletion of either the C-terminal domain or the T1 tetramerization domain of Kctd12.1 raises two possibilities. The first is that the Ulk2 binding site is made up of a portion of both domains. The second is that one domain coordinates the arrangement of the subunits of the tetramer, in order for the other domain to form the binding site. For instance, the binding site for Ulk2 may consist of four C-terminal domains in a particular quartenary structure that is formed only when the tetramerization domain brings four subunits together. Future collaboration with the laboratory of Brandt Eichmann, which specializes in structural biology, may shed light on this question. With help from the Eichmann lab, we have identified several amino acids in the N-terminal oligomerization domain that are both conserved among Kctd12 proteins and predicted by homology modeling to participate in subunit-subunit interactions. Mutation of these residues may lead to an inability of subunits to oligomerize. If the ability of these mutants to form Kctd12.1 complexes in the yeast 2-hybrid system is abolished, testing their ability to bind the Ulk2 PS domain may reveal whether or not the binding domain spans the two domains of an individual Kctd12.1 monomer. If binding of the PS domain simply requires the presence of both N- and C-terminal domains of the Kctd12.1 monomer, we expect the interaction to remain intact even if the formation of Kctd12.1 oligomers is impaired. However, if binding requires, for example, coordination of multiple

Kctd12.1 C-terminal domains by oligomerization, we expect N-terminal oligomerization mutants to also be unable to bind the Ulk2 PS domain.

Ulk2 is thought to promote process extension through stimulation of early endosome trafficking at growing neurite tips. Ulk2 has been shown to increase early endosome formation by activation of the small GTPase Rab5 (Tomoda et al., 2004). In axons, early endosomes that contain activated growth factor receptors (e.g. TrkA bound to NGF) move in a retrograde fashion to the cell body, and this is thought to bring them close enough to the nucleus to allow intracellular signaling to affect transcription and axon extension (Delcroix et al., 2003). A similar process is thought to occur in dendrites, although the receptors and ligands involved remain to be identified (Satoh et al., 2008). We speculate that Kctd12 proteins could regulate this process at a number of steps, but the most likely scenarios involve either a regulation of Ulk2 activity by preventing autophosphorylation or a sequestration model in which Kctd12 proteins inhibit localization of Ulk2 proteins to early endosome signaling centers.

To our knowledge, this is the first reported whole organism knockdown of Ulk2 in a vertebrate model system. Ulk2 is a highly conserved protein from yeast (Atg1) to man, and acts in autophagy as well as early endosome formation. Given the multiple roles of this protein, why do Ulk2 morphants have a relatively mild dendritic outgrowth phenotype in the Hb? First, it is likely that we are only reducing, not eliminating, Ulk2 function in our morpholino-treated embryos, as evidenced by RT-PCR quantification. Second, there is likely some redundancy with the closely related Ulk1a/1b proteins. The selective appearance of an Hb

phenotype may be due to an elevated requirement for Ulk2 in Hb neurons, a conclusion supported by the relatively high levels of *ulk2* transcripts found in these cells.

We have attempted to order the Kctd12/Ulk2 pathway via genetic epistasis. The phenotype of double mutant/morphants is similar to Ulk2 single morphants, and therefore the most parsimonious explanation is that Ulk2 is downstream of Kctd12.1. However, double mutant/morphants do exhibit some increased neuropil relative to Ulk2 morphants, likely because Ulk2 morpholino treatment cannot completely eliminate Ulk2 protein. As higher levels of morpholino are toxic to embryos, we cannot exclude the possibility that Kctd12.1 is downstream of Ulk2 until an *ulk2* null mutation is isolated.

Relative Potency of Kctd12 Proteins as Ulk2 Regulators May Underlie Hb Neuropil Asymmetry

It appears counterintuitive that Hb neurons should express negative regulators of neuropil extension (Kctd12 proteins) given their elaborate dendritic processes. We propose that differential neurite extension among Hb neurons may be controlled by different potencies of Kctd12.1 and Kctd12.2 in the downregulation of Ulk2 activity. The bilateral expression of *ulk2* mRNA suggests that an Ulk2-dependent process is active in all Hb neurons. Asymmetric Kctd12 expression overlaid on symmetric expression of the pro-neurite factor Ulk2 could explain how differential process extension occurs. This model predicts that Kctd12.2 downregulates Ulk2-dependent neuropil outgrowth more effectively than Kctd12.1, resulting in the characteristic asymmetric neuropil observed in the

zebrafish habenulae (Figure 9F). Our data support this model, as overexpression of Kctd12.2 but not Kctd12.1 is able to reduce neuropil volume in all subnuclei, and mutation of Kctd12.2 results in a greater neuropil over-elaboration phenotype than mutation of Kctd12.1.

Since Kctd12.1 and 12.2 are closely related proteins, with ~ 80% similarity at the amino acid level (Gamse et al., 2005), differential ability to affect neuropil formation in the habenular nuclei was unexpected. However, closer inspection of the protein sequences reveals 5 amino acid differences between Kctd12.1 and 12.2 in the C-terminal domain (CTD). As the CTD is essential for Kctd12.1 interaction with Ulk2, these differences may affect the strength of the interaction. Determination of CTD structure at high resolution is underway to identify the residues that contact Ulk2 and reveal the significance of amino acid differences between Kctd12.1 and 12.2. Analysis of the activity of chimeric Kctd12 proteins (that is, Kctd12.1 NTD:Kctd12.2 CTD and vice versa) may help show that sequence divergence in the CTD is responsible for differences in relative potency as Ulk2 regulators.

Kctd12.1-Ulk2 Interaction May Intersect with GABAb Receptor Complexes

Kctd12 (the single mammalian homolog of zebrafish Kctd12.1/12.2) was recently shown to interact with the metabotropic GABAb G-protein coupled receptor. Because the yeast 2-hybrid system involves nuclear localization of proteins, it is inherently unlikely to isolate membrane-localized interactors. Therefore, we were not surprised to have missed GABA receptors as candidates in our screen. This

interaction affects ligand sensitivity, desensitization, and kinetics of this important regulator of synaptic transmission and signal propagation (Schwenk et al., 2010). This result can be interpreted in two possible ways. First, Kctd12 may have distinct roles during the life of a neuron. During embryonic development, Kctd12 may modulate Ulk2-dependent mechanisms of neurite outgrowth, and then regulate electrical activity in mature neurons by an independent interaction with GABAb receptors. In this model, Kctd proteins may switch roles as Hb neurons reach maturity. An Ulk2-dependent neurite growth regulatory system involving Kctd12 proteins may transition to a system in which Kctds fine-tune the dynamics of action potential inhibition by desensitization of GABA complexes. This possibility raises important research questions involving the functional switch from Ulk2 to GABAb regulation. What signal precipitates this change in function? Do Ulk2 and GABAb compete for the same Kctd12 binding site? Future research can determine these answers through basic biochemistry and electrophysiological avenues.

Second, and more intriguingly, we can speculate that the ability of Kctd12 proteins to interact with both Ulk2 and GABAb receptors may reflect a role in GABA-mediated neurite outgrowth. During embryonic development, GABA is known to regulate axon and dendrite formation prior to synapse formation, by activation of GABA receptors, including GABAb receptors (Sernagor et al., 2010). By analogy with NGF/TrkA, internalization of GABA/GABAb receptor complexes into endosomes may affect their signaling properties. Indeed, GABAb receptors in cultured neurons are internalized and recycled via an endosomal pathway,

which appears to be dendrite-specific (Gonzalez-Maeso et al., 2003, Grampp et al., 2008, Vargas et al., 2008). The presence of GABAb receptor-associated Kctd12 could prevent Ulk2-stimulated endocytosis of the receptor, or affect the recycling of GABAb-receptor-containing endosomes to the cell surface versus targeting to the proteasome. The discovery and characterization of GABAb/Ulk2/Kctd complexes would be a truly novel finding, and may lead to important new insights into developmental processes that give rise to functional regulation of mature neurons.

Behavioral Consequences of Improper Hb Development

The habenulo-interpeduncular conduction pathway is a central link between neurons of the forebrain and midbrain. In humans, habenular neurons connect the sensory and executive regions of the cortex with the brainstem. Hence, it is no surprise that habenular disfunction has been linked to anxiety and depression, and that as part of the brain's reward system, cocaine and nicotine addiction is known to destroy Hb neurons. Studies in mammals using lesions of Hb output, the fasciculus retroflexus, indicate a strong role for functional Hb neurons in behaviors as diverse as sleep, reward-based learning, fear, anxiety, and depression. It seems that Hb neurons are able to regulate both serotonergic and dopaminergic systems, suggesting that the Hb functions at a crossroad of behavioral control (Hikosaka, 2010).

Habenular conduction has also been shown to be active during decisions-making tasks in primates. Neurons of the macaque lateral Hb were excited by

the appearance of a smaller-than-expected reward, and inhibited by the appearance of a large reward. The response of downstream dopaminergic neurons controlling movement were opposite to this trend. These data suggest that activation of Hb neurons in response to a small reward inhibits the dopaminergic system, and consequently leading to less physical movement. In this way, the Hb can be thought of as an integral part of the reward-based learning process (Matsumoto and Hikosaka, 2007).

The Hb also have a described role in the generation of stress-induced behaviors. Hb neurons are excited in monkeys following repeated exposure to aversive stimuli, and characteristic suppression of motor behavior in stress-induced “helpless” animals is also thought to be caused by suppression of dopaminergic neurons by Hb activation (Matsumoto and Hikosaka, 2009). Indeed, long periods of inescapable aversive stimuli are capable of sensitizing Hb neurons, leading to continuously elevated activity and behavioral changes including suppression of motor activity. It is not clear whether the serotonergic or dopaminergic pathways are responsible for depressive behavior, but clearly, Hb activity is involved (Hikosaka, 2010).

Recent behavioral experiments in zebrafish analyzing the relationship between anxiety and fear response suggest that the habenulo-interpeduncular conduction pathway may be responsible for termination of the anxiety response and the ability of individuals to engage in escape responses after conditioning (Jesuthasan, 2011). In two studies, genetic abrogation of Hb function leads to defects in the escape response to a conditioned stimulus. In both larvae (Lee et

al., 2010) and adults (Agetsuma et al., 2010) disruption of Hb function leads to an inability to continue to avoid a conditioned shock stimulus. When normal zebrafish are conditioned to expect a shock in response to a visual stimulus, they attempt to escape by increase in speed and turn rate, or if the shock is localized and escapeable, by crossing into the opposite end of the tank. In contrast, when Hb neurons are compromised, animals tend to freeze and are generally unable to initiate the escape response. In fact, this behavior is similar to observations of models of anxiety in which fish are conditioned to an inescapable shock. The authors of these studies conclude that Hb neurons are required for the modification of the fear response based on experience.

The development of an effective assay for Hb disfunction may be an entry point by which we can further define the consequences of inappropriate development of the Hb, and discover possible roles for Kctd proteins in the functioning adult brain. One research direction suggested by the work presented here is the evaluation of similar behavioral defects in animals with Hb neuropil defects caused by manipulation of Kctd12 or Ulk2 expression. Additionally, the described role of Kctd12 proteins in modulation of GABA receptor function could significantly impact the ability of fish to initiate the escape response.

Bringing these behavioral discoveries together with the finding that Kctd12 proteins may regulate firing inhibition by GABAb receptors offers intriguing possibilities for future research. GABAergic systems are known to be involved in the generation of anxiety and depressive behaviors (Cryan and Slattery, 2010). Indeed, the behavioral response of GABA(B1))-/- mice in anxiety tests are very

similar to the behavior of zebrafish in the absence of the habenular conduction system (Mombereau et al., 2004, Lee et al., 2010). Now that behavioral assays have been developed for analysis of Hb disfunction, the role of Kctd12 proteins in generating the relevant behaviors can be relatively easily determined. The most obvious open question is whether or not a detectable reduction in escape response can be elicited by simply removing Kctd12.1 and Kctd12.2 from the functioning adult brain. Here we have shown that the mutation of Kctd12 proteins leads to subtle overdevelopment of Hb neuropil, but future research should focus on whether this neuropil overdevelopment can lead directly to a behavioral phenotype in a conditioned response environment, or if there is separate role for Kctds in adult neurons. Using existing behavioral assays to test the response of Kctd12 mutants will be the first step to determining whether or not they play an active role in the regulation of broad behavioral responses.

REFERENCES

Agetsuma M, Aizawa H, Aoki T, Nakayama R, Takahoko M, Goto M, Sassa T, Amo R, Shiraki T, Kawakami K, Hosoya T, Higashijima S, Okamoto H (2010) The habenula is crucial for experience-dependent modification of fear responses in zebrafish. Nat Neurosci 13:1354-1356.

Ahmad N, Long S, Rebagliati M (2004) A southpaw joins the roster: the role of the zebrafish nodal-related gene southpaw in cardiac LR asymmetry. Trends Cardiovasc Med 14:43-49.

Aizawa H, Bianco IH, Hamaoka T, Miyashita T, Uemura O, Concha ML, Russell C, Wilson SW, Okamoto H (2005) Laterotopic representation of left-right information onto the dorso-ventral axis of a zebrafish midbrain target nucleus. Curr Biol 15:238-243.

Aizawa H, Goto M, Sato T, Okamoto H (2007) Temporally regulated asymmetric neurogenesis causes left-right difference in the zebrafish habenular structures. Dev Cell 12:87-98.

Amsterdam A, Burgess S, Golling G, Chen W, Sun Z, Townsend K, Farrington S, Haldi M, Hopkins N (1999) A large-scale insertional mutagenesis screen in zebrafish. Genes Dev 13:2713-2724.

Asai T, Sugimori E, Tanno Y (2009) Schizotypal personality traits and atypical lateralization in motor and language functions. Brain Cogn 71:26-37.

Barkovich AJ, Hevner R, Guerrini R (1999) Syndromes of bilateral symmetrical polymicrogyria. AJNR Am J Neuroradiol 20:1814-1821.

Barth KA, Miklosi A, Watkins J, Bianco IH, Wilson SW, Andrew RJ (2005) fsi zebrafish show concordant reversal of laterality of viscera, neuroanatomy, and a subset of behavioral responses. Curr Biol 15:844-850.

Bianco IH, Carl M, Russell C, Clarke JD, Wilson SW (2008) Brain asymmetry is encoded at the level of axon terminal morphology. Neural Dev 3:9.

Bisgrove BW, Essner JJ, Yost HJ (2000) Multiple pathways in the midline regulate concordant brain, heart and gut left-right asymmetry. Development 127:3567-3579.

Bisgrove BW, Morelli SH, Yost HJ (2003) Genetics of human laterality disorders: insights from vertebrate model systems. Annu Rev Genomics Hum Genet 4:1-32.

Bleich-Cohen M, Hendler T, Kotler M, Strous RD (2009) Reduced language lateralization in first-episode schizophrenia: an fMRI index of functional asymmetry. Psychiatry Res 171:82-93.

Braitenberg V, Kemali M (1970) Exceptions to bilateral symmetry in the epithalamus of lower vertebrates. J Comp Neurol 138:137-146.

Brueckner M (2007) Heterotaxia, congenital heart disease, and primary ciliary dyskinesia. Circulation 115:2793-2795.

Cahill GM (1996) Circadian regulation of melatonin production in cultured zebrafish pineal and retina. Brain Res 708:177-181.

Carl M, Bianco IH, Bajoghli B, Aghaallaei N, Czerny T, Wilson SW (2007) Wnt/Axin1/beta-catenin signaling regulates asymmetric nodal activation, elaboration, and concordance of CNS asymmetries. Neuron 55:393-405.

Chang BS, Apse KA, Caraballo R, Cross JH, McLellan A, Jacobson RD, Valente KD, Barkovich AJ, Walsh CA (2006) A familial syndrome of unilateral polymicrogyria affecting the right hemisphere. Neurology 66:133-135.

Chi JG, Dooling EC, Gilles FH (1977) Gyral development of the human brain. Ann Neurol 1:86-93.

Concha ML, Burdine RD, Russell C, Schier AF, Wilson SW (2000) A nodal signaling pathway regulates the laterality of neuroanatomical asymmetries in the zebrafish forebrain. Neuron 28:399-409.

Concha ML, Russell C, Regan JC, Tawk M, Sidi S, Gilmour DT, Kapsimali M, Sumoy L, Goldstone K, Amaya E, Kimelman D, Nicolson T, Grunder S, Gomperts M, Clarke JD, Wilson SW (2003) Local tissue interactions across the dorsal midline of the forebrain establish CNS laterality. Neuron 39:423-438.

Concha ML, Wilson SW (2001) Asymmetry in the epithalamus of vertebrates. J Anat 199:63-84.

Crow TJ, Ball J, Bloom SR, Brown R, Bruton CJ, Colter N, Frith CD, Johnstone EC, Owens DG, Roberts GW (1989) Schizophrenia as an anomaly of development of cerebral asymmetry. A postmortem study and a proposal concerning the genetic basis of the disease. Arch Gen Psychiatry 46:1145-1150.

Cryan JF, Slattery DA (2010) GABAB receptors and depression. Current status. Adv Pharmacol 58:427-451.

Delcroix JD, Valletta JS, Wu C, Hunt SJ, Kowal AS, Mobley WC (2003) NGF signaling in sensory neurons: evidence that early endosomes carry NGF retrograde signals. Neuron 39:69-84.

Dementieva IS, Tereshko V, McCrossan ZA, Solomaha E, Araki D, Xu C, Grigorieff N, Goldstein SA (2009) Pentameric assembly of potassium channel tetramerization domain-containing protein 5. J Mol Biol 387:175-191.

Draper BW, McCallum CM, Stout JL, Slade AJ, Moens CB (2004) A high-throughput method for identifying N-ethyl-N-nitrosourea (ENU)-induced point mutations in zebrafish. Methods Cell Biol 77:91-112.

Duara R, Kushch A, Gross-Glenn K, Barker WW, Jallad B, Pascal S, Loewenstein DA, Sheldon J, Rabin M, Levin B, al. e (1991) Neuroanatomic differences between dyslexic and normal readers on magnetic resonance imaging scans. Arch Neurol 48:410-416.

Essner JJ, Vogan KJ, Wagner MK, Tabin CJ, Yost HJ, Brueckner M (2002) Conserved function for embryonic nodal cilia. Nature 418:37-38.

Facchin L, Burgess HA, Siddiqi M, Granato M, Halpern ME (2009) Determining the function of zebrafish epithalamic asymmetry. Philos Trans R Soc Lond B Biol Sci 364:1021-1032.

Fischer A, Viebahn C, Blum M (2002) FGF8 acts as a right determinant during establishment of the left-right axis in the rabbit. Curr Biol 12:1807-1816.

Galaburda AM, Sherman GF, Rosen GD, Aboitiz F, Geschwind N (1985) Developmental dyslexia: four consecutive patients with cortical anomalies. Ann Neurol 18:222-233.

Gamse JT, Kuan YS, Macurak M, Brosamle C, Thisse B, Thisse C, Halpern ME (2005) Directional asymmetry of the zebrafish epithalamus guides dorsoventral innervation of the midbrain target. Development 132:4869-4881.

Gamse JT, Shen YC, Thisse C, Thisse B, Raymond PA, Halpern ME, Liang JO (2002) Otx5 regulates genes that show circadian expression in the zebrafish pineal complex. Nat Genet 30:117-121.

Gamse JT, Thisse C, Thisse B, Halpern ME (2003) The parapineal mediates left-right asymmetry in the zebrafish diencephalon. Development 130:1059-1068.

Geschwind N, Levitsky W (1968) Human brain: left-right asymmetries in temporal speech region. Science 161:186-187.

Gonzalez-Maeso J, Wise A, Green A, Koenig JA (2003) Agonist-induced desensitization and endocytosis of heterodimeric GABAB receptors in CHO-K1 cells. Eur J Pharmacol 481:15-23.

Gothilf Y, Coon SL, Toyama R, Chitnis A, Namboodiri MA, Klein DC (1999) Zebrafish serotonin N-acetyltransferase-2: marker for development of pineal photoreceptors and circadian clock function. Endocrinology 140:4895-4903.

Grampp T, Notz V, Broll I, Fischer N, Benke D (2008) Constitutive, agonist-accelerated, recycling and lysosomal degradation of GABA(B) receptors in cortical neurons. Mol Cell Neurosci 39:628-637.

Hamill GS, Lenn NJ (1984) The subnuclear organization of the rat interpeduncular nucleus: a light and electron microscopic study. J Comp Neurol 222:396-408.

Harris JA, Guglielmotti V, Bentivoglio M (1996) Diencephalic asymmetries. Neurosci Biobehav Rev 20:637-643.

Hendricks M, Jesuthasan S (2007) Asymmetric innervation of the habenula in zebrafish. J Comp Neurol 502:611-619.

Hikosaka O (2010) The habenula: from stress evasion to value-based decision-making. Nat Rev Neurosci 11:503-513.

Humphreys P, Kaufmann WE, Galaburda AM (1990) Developmental dyslexia in women: neuropathological findings in three patients. Ann Neurol 28:727-738.

Hynd GW, Semrud-Clikeman M, Lorys AR, Novey ES, Eliopulos D (1990) Brain morphology in developmental dyslexia and attention deficit disorder/hyperactivity. Arch Neurol 47:919-926.

Inbal A, Kim SH, Shin J, Solnica-Krezel L (2007) Six3 represses nodal activity to establish early brain asymmetry in zebrafish. Neuron 55:407-415.

Jeon YW, Polich J (2001) P300 asymmetry in schizophrenia: a meta-analysis. Psychiatry Res 104:61-74.

Jesuthasan S (2011) Fear, anxiety and control in the zebrafish. Dev Neurobiol.

Kennedy DN, O'Craven KM, Ticho BS, Goldstein AM, Makris N, Henson JW (1999) Structural and functional brain asymmetries in human situs inversus totalis. Neurology 53:1260-1265.

Kuan YS, Yu HH, Moens CB, Halpern ME (2007) Neuropilin asymmetry mediates a left-right difference in habenular connectivity. Development 134:857-865.

Kushch A, Gross-Glenn K, Jallad B, Lubs H, Rabin M, Feldman E, Duara R (1993) Temporal lobe surface area measurements on MRI in normal and dyslexic readers. Neuropsychologia 31:811-821.

Kwan KM, Fujimoto E, Grabher C, Mangum BD, Hardy ME, Campbell DS, Parant JM, Yost HJ, Kanki JP, Chien CB (2007) The Tol2kit: a multisite gateway-based construction kit for Tol2 transposon transgenesis constructs. Dev Dyn 236:3088-3099.

Larsen JP, Hoien T, Lundberg I, Odegaard H (1990) MRI evaluation of the size and symmetry of the planum temporale in adolescents with developmental dyslexia. Brain Lang 39:289-301.

Lee A, Mathuru AS, Teh C, Kibat C, Korzh V, Penney TB, Jesuthasan S (2010) The habenula prevents helpless behavior in larval zebrafish. Curr Biol 20:2211-2216.

Lein ES, Hawrylycz MJ, Ao N, Ayres M, Bensinger A, Bernard A, Boe AF, Boguski MS, Brockway KS, Byrnes EJ, Chen L, Chen TM, Chin MC, Chong J, Crook BE, Czaplinska A, Dang CN, Datta S, Dee NR, Desaki AL, Desta T, Diep E, Dolbeare TA, Donelan MJ, Dong HW, Dougherty JG,

Duncan BJ, Ebbert AJ, Eichele G, Estin LK, Faber C, Facer BA, Fields R, Fischer SR, Fliss TP, Frensley C, Gates SN, Glattfelder KJ, Halverson KR, Hart MR, Hohmann JG, Howell MP, Jeung DP, Johnson RA, Karr PT, Kawal R, Kidney JM, Knapik RH, Kuan CL, Lake JH, Laramee AR, Larsen KD, Lau C, Lemon TA, Liang AJ, Liu Y, Luong LT, Michaels J, Morgan JJ, Morgan RJ, Mortrud MT, Mosqueda NF, Ng LL, Ng R, Orta GJ, Overly CC, Pak TH, Parry SE, Pathak SD, Pearson OC, Puchalski RB, Riley ZL, Rockett HR, Rowland SA, Royall JJ, Ruiz MJ, Sarno NR, Schaffnit K, Shapovalova NV, Sivisay T, Slaughterbeck CR, Smith SC, Smith KA, Smith BI, Sodt AJ, Stewart NN, Stumpf KR, Sunkin SM, Sutram M, Tam A, Teemer CD, Thaller C, Thompson CL, Varnam LR, Visel A, Whitlock RM, Wohnoutka PE, Wolkey CK, Wong VY, Wood M, Yaylaoglu MB, Young RC, Youngstrom BL, Yuan XF, Zhang B, Zwingman TA, Jones AR (2007) Genome-wide atlas of gene expression in the adult mouse brain. Nature 445:168-176.

LeMay M (1976) Morphological cerebral asymmetries of modern man, fossil man, and nonhuman primate. Ann N Y Acad Sci 280:349-366.

Lennox BR, Park SB, Jones PB, Morris PG (1999) Spatial and temporal mapping of neural activity associated with auditory hallucinations. Lancet 353:644.

Levin M (2004) The embryonic origins of left-right asymmetry. Crit Rev Oral Biol Med 15:197-206.

Levin M, Johnson RL, Stern CD, Kuehn M, Tabin C (1995) A molecular pathway determining left-right asymmetry in chick embryogenesis. Cell 82:803-814.

Liang JO, Etheridge A, Hantsoo L, Rubinstein AL, Nowak SJ, Izpisua Belmonte JC, Halpern ME (2000) Asymmetric nodal signaling in the zebrafish diencephalon positions the pineal organ. Development 127:5101-5112.

Long S, Ahmad N, Rebagliati M (2003) The zebrafish nodal-related gene southpaw is required for visceral and diencephalic left-right asymmetry. Development 130:2303-2316.

Lowe LA, Supp DM, Sampath K, Yokoyama T, Wright CV, Potter SS, Overbeek P, Kuehn MR (1996) Conserved left-right asymmetry of nodal expression and alterations in murine situs inversus. Nature 381:158-161.

Lyttelton OC, Karama S, Ad-Dab'bagh Y, Zatorre RJ, Carbonell F, Worsley K, Evans AC (2009) Positional and surface area asymmetry of the human cerebral cortex. Neuroimage 46:895-903.

MacNeilage PF, Rogers LJ, Vallortigara G (2009) Origins of the left & right brain. Sci Am 301:60-67.

Matsumoto M, Hikosaka O (2007) Lateral habenula as a source of negative reward signals in dopamine neurons. Nature 447:1111-1115.

Matsumoto M, Hikosaka O (2009) Two types of dopamine neuron distinctly convey positive and negative motivational signals. Nature 459:837-841.

McGrath J, Brueckner M (2003) Cilia are at the heart of vertebrate left-right asymmetry. Curr Opin Genet Dev 13:385-392.

Miyasaka N, Morimoto K, Tsubokawa T, Higashijima S, Okamoto H, Yoshihara Y (2009) From the olfactory bulb to higher brain centers: genetic

visualization of secondary olfactory pathways in zebrafish. J Neurosci 29:4756-4767.

Moffat SD, Hampson E, Lee DH (1998) Morphology of the planum temporale and corpus callosum in left handers with evidence of left and right hemisphere speech representation. Brain 121 (Pt 12):2369-2379.

Mombereau C, Kaupmann K, Froestl W, Sansig G, van der Putten H, Cryan JF (2004) Genetic and pharmacological evidence of a role for GABA(B) receptors in the modulation of anxiety- and antidepressant-like behavior. Neuropsychopharmacology 29:1050-1062.

Morgan AE, Hynd GW (1998) Dyslexia, neurolinguistic ability, and anatomical variation of the planum temporale. Neuropsychol Rev 8:79-93.

Ogura K, Wicky C, Magnenat L, Tobler H, Mori I, Muller F, Ohshima Y (1994) Caenorhabditis elegans unc-51 gene required for axonal elongation encodes a novel serine/threonine kinase. Genes Dev 8:2389-2400.

Ohi Y, Wright CV (2007) Anteriorward shifting of asymmetric Xnr1 expression and contralateral communication in left-right specification in Xenopus. Dev Biol 301:447-463.

Palmer AR (2004) Selection for asymmetry. Science 306:812-813; author reply 812-813.

Pascual-Castroviejo I, Pascual-Pascual SI, Viano J, Martinez V, Palencia R (2001) Unilateral polymicrogyria: a common cause of hemiplegia of prenatal origin. Brain Dev 23:216-222.

Paukert M, Sidi S, Russell C, Siba M, Wilson SW, Nicolson T, Grunder S (2004) A family of acid-sensing ion channels from the zebrafish: widespread expression in the central nervous system suggests a conserved role in neuronal communication. J Biol Chem 279:18783-18791.

Petty RG (1999) Structural asymmetries of the human brain and their disturbance in schizophrenia. Schizophr Bull 25:121-139.

Ranft K, Dobrowolny H, Krell D, Bielau H, Bogerts B, Bernstein HG (2009) Evidence for structural abnormalities of the human habenular complex in affective disorders but not in schizophrenia. Psychol Med 1-11.

Regan JC, Concha ML, Roussigne M, Russell C, Wilson SW (2009) An Fgf8-dependent bistable cell migratory event establishes CNS asymmetry. Neuron 61:27-34.

Roussigne M, Bianco IH, Wilson SW, Blader P (2009) Nodal signalling imposes left-right asymmetry upon neurogenesis in the habenular nuclei. Development 136:1549-1557.

Sann S, Wang Z, Brown H, Jin Y (2009) Roles of endosomal trafficking in neurite outgrowth and guidance. Trends Cell Biol 19:317-324.

Satoh D, Sato D, Tsuyama T, Saito M, Ohkura H, Rolls MM, Ishikawa F, Uemura T (2008) Spatial control of branching within dendritic arbors by dynein-dependent transport of Rab5-endosomes. Nat Cell Biol 10:1164-1171.

Schwenk J, Metz M, Zolles G, Turecek R, Fritzius T, Bildl W, Tarusawa E, Kulik A, Unger A, Ivankova K, Seddik R, Tiao JY, Rajalu M, Trojanova J, Rohde V, Gassmann M, Schulte U, Fakler B, Bettler B (2010) Native GABA(B)

receptors are heteromultimers with a family of auxiliary subunits. Nature 465:231-235.

Scott EK, Mason L, Arrenberg AB, Ziv L, Gosse NJ, Xiao T, Chi NC, Asakawa K, Kawakami K, Baier H (2007) Targeting neural circuitry in zebrafish using GAL4 enhancer trapping. Nat Methods 4:323-326.

Sernagor E, Chabrol F, Bony G, Cancedda L (2010) GABAergic control of neurite outgrowth and remodeling during development and adult neurogenesis: general rules and differences in diverse systems. Front Cell Neurosci 4:11.

Shen MM (2007) Nodal signaling: developmental roles and regulation. Development 134:1023-1034.

Shepard PD, Holcomb HH, Gold JM (2006) Schizophrenia in translation: the presence of absence: habenular regulation of dopamine neurons and the encoding of negative outcomes. Schizophr Bull 32:417-421.

Shiratori H, Hamada H (2006) The left-right axis in the mouse: from origin to morphology. Development 133:2095-2104.

Snelson CD, Gamse JT (2009) Building an asymmetric brain: development of the zebrafish epithalamus. Semin Cell Dev Biol 20:491-497.

Snelson CD, Santhakumar K, Halpern ME, Gamse JT (2008) Tbx2b is required for the development of the parapineal organ. Development 135:1693-1702.

Solnica-Krezel L (2003) Vertebrate development: taming the nodal waves. Curr Biol 13:R7-9.

Soroldoni D, Bajoghli B, Aghaallaei N, Czerny T (2007) Dynamic expression pattern of Nodal-related genes during left-right development in medaka. Gene Expr Patterns 7:93-101.

Steinmetz H (1996) Structure, functional and cerebral asymmetry: in vivo morphometry of the planum temporale. Neurosci Biobehav Rev 20:587-591.

Sutherland RJ (1982) The dorsal diencephalic conduction system: a review of the anatomy and functions of the habenular complex. Neurosci Biobehav Rev 6:1-13.

Thisse C, Thisse B (2008) High-resolution in situ hybridization to whole-mount zebrafish embryos. Nat Protoc 3:59-69.

Thompson PM, Hayashi KM, de Zubicaray G, Janke AL, Rose SE, Semple J, Herman D, Hong MS, Dittmer SS, Doddrell DM, Toga AW (2003) Dynamics of gray matter loss in Alzheimer's disease. J Neurosci 23:994-1005.

Toda H, Mochizuki H, Flores R, 3rd, Josowitz R, Krasieva TB, Lamorte VJ, Suzuki E, Gindhart JG, Furukubo-Tokunaga K, Tomoda T (2008) UNC-51/ATG1 kinase regulates axonal transport by mediating motor-cargo assembly. Genes Dev 22:3292-3307.

Toga AW, Thompson PM (2003) Mapping brain asymmetry. Nat Rev Neurosci 4:37-48.

Tomoda T, Kim JH, Zhan C, Hatten ME (2004) Role of Unc51.1 and its binding partners in CNS axon outgrowth. Genes Dev 18:541-558.

Tubbs RS, Wellons JC, 3rd, Salter G, Blount JP, Oakes WJ (2003) Intracranial anatomic asymmetry in situs inversus totalis. Anat Embryol (Berl) 206:199-202.

Vargas KJ, Terunuma M, Tello JA, Pangalos MN, Moss SJ, Couve A (2008) The availability of surface GABA B receptors is independent of gamma-aminobutyric acid but controlled by glutamate in central neurons. J Biol Chem 283:24641-24648.

Walker C (1999) Haploid screens and gamma-ray mutagenesis. Methods Cell Biol 60:43-70.

Westerfield M, ZFIN. (2000) The zebrafish book a guide for the laboratory use of zebrafish Danio (Brachydanio) rerio. Eugene, Or.: ZFIN.

Yan J, Kuroyanagi H, Tomemori T, Okazaki N, Asato K, Matsuda Y, Suzuki Y, Ohshima Y, Mitani S, Masuho Y, Shirasawa T, Muramatsu M (1999) Mouse ULK2, a novel member of the UNC-51-like protein kinases: unique features of functional domains. Oncogene 18:5850-5859.

Zhou X, Babu JR, da Silva S, Shu Q, Graef IA, Oliver T, Tomoda T, Tani T, Wooten MW, Wang F (2007) Unc-51-like kinase 1/2-mediated endocytic processes regulate filopodia extension and branching of sensory axons. Proc Natl Acad Sci U S A 104:5842-5847.